

# Special Issue: *Australopithecus sediba*

## The Pelvis of *Australopithecus sediba*

STEVEN E. CHURCHILL

Department of Evolutionary Anthropology, Box 90383, Duke University, Durham, NC 27708, USA; and, Evolutionary Studies Institute, University of the Witwatersrand, Private Bag 3, Wits 2050, Johannesburg, SOUTH AFRICA; [churchy@duke.edu](mailto:churchy@duke.edu)

JOB M. KIBII

Division of Palaeontology and Palaeoanthropology, National Museums of Kenya, PO Box 40658-00100, KENYA; and, Evolutionary Studies Institute, University of the Witwatersrand, Private Bag 3, Wits 2050, Johannesburg, SOUTH AFRICA; [jobkibii@hotmail.com](mailto:jobkibii@hotmail.com)

PETER SCHMID

Anthropological Institute and Museum, University of Zurich, Winterthurerstr. 190, CH-8057 Zurich, SWITZERLAND; and, Evolutionary Studies Institute, University of the Witwatersrand, Private Bag 3, Wits 2050, Johannesburg, SOUTH AFRICA; [peterschmid2014@gmail.com](mailto:peterschmid2014@gmail.com)

NICHELE D. REED

Natural History Museum of Utah, 301 Wakara Way, Salt Lake City, Utah 84108, USA; [nosaurus@nhmu.utah.edu](mailto:nosaurus@nhmu.utah.edu)

LEE R. BERGER

Evolutionary Studies Institute, University of the Witwatersrand, Private Bag 3, Wits 2050, Johannesburg, SOUTH AFRICA; [profleeberger@yahoo.com](mailto:profleeberger@yahoo.com)

submitted: 17 November 2017; accepted 27 July 2018

### ABSTRACT

Pelvic remains of two individuals of *Australopithecus sediba*—a subadult male (MH1) and an adult female (MH2)—have been recovered from early Pleistocene deposits at Malapa Cave in Gauteng Province, South Africa. The pelvis of MH1 is represented by partial right and left ilia, a left ischium, and the left pubic symphysis, while that of MH2 is represented by a partial right os coxae (lacking the ischium and a portion of the iliac blade), a fragmentary left pubis, and a partial sacrum. Together these remains document pelvic morphology that was similar in some respects to that of other known species of *Australopithecus* (e.g., in having relatively small sacral and acetabular joint surfaces, a relatively long pubis, and, in at least one individual, an anteriorly positioned and weakly developed acetabulocrystal buttress), while being more like that of most species of the genus *Homo* in others (e.g., in having greater sigmoid curvature and a more sagittal orientation of the iliac blades, increased buttressing of the lower iliac body [acetabulosacral buttress], and a shortened ischium with a narrow tuberoacetabular sulcus). This mosaic of australopith-like and *Homo*-like morphology in the pelvis of *Au. sediba* parallels the morphological pattern seen throughout the cranial and postcranial skeleton of this late australopith.

This special issue is guest-edited by Scott A. Williams (Department of Anthropology, New York University) and Jeremy M. DeSilva (Department of Anthropology, Dartmouth College). This is article #6 of 9.

### INTRODUCTION

Remains of the ossa coxae of both the subadult male specimen Malapa Hominin 1 (MH1) and the adult female specimen Malapa Hominin 2 (MH2) have been recovered to date, but the sacrum is currently known only from MH2. The pelvis of MH1 is represented by a partial right ilium (itself composed of two conjoining fragments), a partial left

ilium, a left ischium, and a small fragment of the left pubic body. The triradiate cartilage of the left os coxae was patent in MH1 (that is, the ischium was unfused to the ilium), consistent with his subadult age at death. The pelvis of MH2 consists of a partial right ilium, right pubis, partial sacrum, and a fragment of the left pubic body. Although fragmentary, both pelvises are sufficiently complete so as to allow



Figure 1. Fragments of the right ilium of MH1. Top row: U.W. 88-6 in internal (right) and external (left) perspectives; Bottom row: U.W. 88-7 in internal (right) and external (left) perspectives (scale bar in centimeters).

reconstruction (Kibii et al. 2011). These remains have added considerably to our understanding of morphological diversity in the hip of small-brained, small-bodied australopiths, and have raised new questions about the adaptive meaning of the morphological differences that separate the pelvis of most australopiths from those of most members of the genus *Homo* (Berger et al. 2010; Kibii et al. 2011). Here we provide detailed morphological descriptions of each element by individual, followed by brief discussion of pelvic morphology in *Au. sediba* relative to that of known hominin species in the genera *Australopithecus* and *Homo*. Printable, 3D surface scans of all of the fossils described in this paper can be found on MorphoSource ([www.morphosource.org](http://www.morphosource.org)) under the project heading “*Australopithecus sediba*.”

## OSSA COXAE

### OSSA COXAE OF MALAPA HOMININ 1 (MH1)

#### U.W. 88-6/7: Partial Right Ilium

**Preservation.** The right ilium of MH1 is represented by two conjoining fragments (Figure 1). Matrix adhering to the broken edges prevents the physical refitting of the two pieces, but with virtual cleaning of the surfaces their ap-

position is readily confirmed (Figure 2). The larger of the two iliac fragments (U.W. 88-7) measures 77mm x 43mm in superoinferior (SI) and anteroposterior (AP) dimensions, respectively. This fragment preserves the greater sciatic notch, the auricular surface, and the posterior inferior iliac spine (PIIS), along with much of the iliac body (including the arcuate line). The larger fragment also preserves approximately 14mm of the iliac tuberosity superior to the auricular surface, as well as the dorsal portion (15mm in a mediolateral dimension) of the iliac fossa. It also retains the posterior margin of the ilium as a continuous surface beginning from a point superior to the ilioischial junction and extending superiorly to a point immediately inferior to the posterior superior iliac spine (PSIS). The smaller of the two iliac fragments (U.W. 88-6) measures 56mm x 40mm in SI and AP dimensions, respectively. This smaller fragment preserves the iliac contribution to the acetabulum, the anterior-most portion of the epiphyseal surface for the pubis, and the posterior-most portion of the epiphyseal surface for the ischium. This fragment also retains the anterior margin of the iliac blade beginning from a point inferior to the anterior superior iliac spine (ASIS) and extending inferiorly to include the anterior inferior iliac spine (AIIS) and the anterior margin of the acetabulum. In the developing os

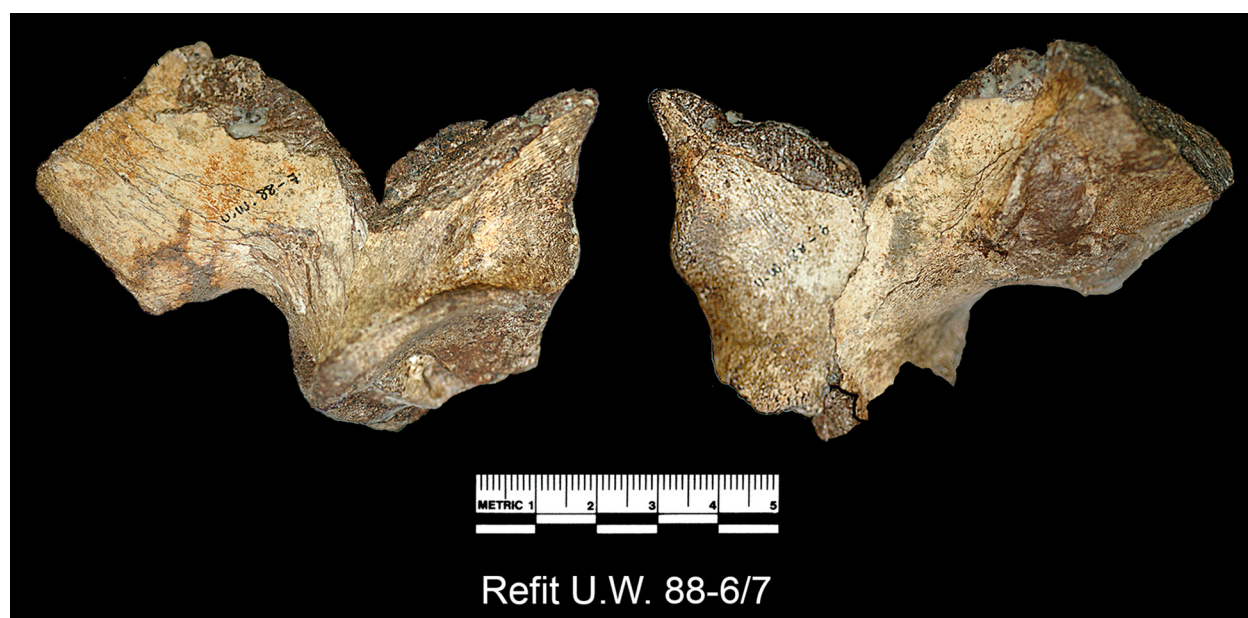


Figure 2. Fragmentary right ilium of MH1 formed by refitting U.W. 88-6 and U.W. 88-7 in internal (right) and external (left) perspectives. Note that the conjoined ilium is rotated slightly laterally relative to the perspective in Figure 1 (scale bar in centimeters).

coxae, the articular subchondral bone of the lunate surface forms from three separate secondary centers associated with the triradiate cartilage—the os acetabulum forms the pubic contribution, while separate acetabular epiphyses associated with the ilium and ischium form their respective contributions (Ponseti 1978). In U.W. 88-6 the acetabular roof appears to be comprised of subchondral bone, indicating that the iliac acetabular epiphysis had fused to the iliac body by the time of death of MH1.

On the larger fragment (U.W. 88-7), fine cracks extending in a superoinferior direction adorn the posterior iliac fossa just ventral of the auricular surface, and interrupt the arcuate line inferiorly. Similar cracks are present on the dorsal side of the preserved portion of the iliac blade. A small patch of cortical bone (ca. 12mm AP by 10mm SI) has exfoliated from the dorsal side of the blade adjacent to the greater sciatic notch. Matrix adheres to all of the broken margins of the larger fragment. A small crack runs through the acetabular surface of the smaller fragment (U.W. 88-6) in an anterosuperior to posteroinferior direction. A large oval pit, measuring 15mm x 7mm in anteroposterior (AP) and mediolateral (ML) dimensions, respectively, marks the medial margin of the lunate surface on the smaller fragment.

None of the iliac crest is present on either fragment, and thus it is not possible to determine if the crest was fused. It appears that the secondary center of ossification for the AIIS was unfused or was only partially fused (the superior part of the spine has a texture consistent with an unfused apophyseal surface), and that matrix has infilled the depressed apophyseal attachment area.

**Morphology.** The auricular surface is L-shaped, with the long axis of the upper limb of the auricular surface being roughly perpendicular to the long axis of the low-

er limb. The upper limb has a length (SA-IP diameter) of 21.5mm and an average width ([minimum + maximum IA-SP diameter]/2) of 14.1mm. The lower limb has a length (apex to PIIS: IA-SP) of 32.1mm and an average height ([minimum + maximum SA-IP diameter]/2) of 13.9mm, for a total auricular area (Kibii et al. 2011 SOM) of 553.3mm<sup>2</sup>. A very slight preauricular sulcus is present. There is some slight rugosity on the preauricular surface (adjacent to the greater sciatic notch and inferior to the auricular surface) in the area of the superior-most line of attachment of *M. obturator internus*. When the fragment is held in anatomical position, the anterior corner of the auricular surface lies ca. 5mm anterior of the greater sciatic notch. This feature is sexually dimorphic in living humans (in females the anterior margin of the auricular surface tends to fall posterior of the sciatic notch: Arsuaga and Alonso 1983). Arsuaga and Alonso (1983) noted that all of the australopiths they studied exhibited the female pattern, and concluded that taxonomic differences existed in the expression of the trait. The MH1 right ilium (as well as the left: see below), however, shows the male pattern.

The postauricular surface preserves a portion of the iliac tuberosity as two large, rugose tubercles. The larger of the two is posterior, its most projecting point lying 14.2mm above the superior margin of the posterior part of the auricular surface, and about 10mm anterior of the posterior margin of the ilium. The smaller tubercle is the more rugose, and it lies 17.0mm above the superior margin of the posterior part of the auricular surface, and about 24mm anterior of the posterior margin of the ilium. The size and morphology of the iliac tuberosity suggests hypertrophy of the posterior interosseous sacroiliac ligament relative to the condition seen in australopith specimens A.L. 288-1 and Sts 14. The posterior margin of the ilium between the PSIS

TABLE 1. MEASUREMENTS USED IN COMPARATIVE ANALYSIS.\*

Abbreviation	Measurement	Definition
ICPA	Iliac crest posterior angle (at spina limitans)	Angle formed between the anterior and posterior portions of the iliac crest, at the spina limitans (determined geometrically following Kibii et al. 2011 SOM)
ICAA	Iliac crest anterior angle (at cristal tubercle)	Angle formed between the anterior and posterior portions of the iliac crest, at the cristal tubercle, or at the lateral-most point on iliac crest in australopiths (determined geometrically following Kibii et al. 2011 SOM)
IA	Iliac angle	Angle formed, in the plane of the pubic body, between a line connecting the most anterosuperior point of the pubic symphysis to the center of the acetabulum with a line drawn through the ASIS and AIIS (taken with protractor on reconstructed pelvis: see Kibii et al. 2011 SOM).
ASLA	Acetabulosacral load arm	Minimum distance from the apex of the auricular surface to the lunate surface of the acetabulum (taken with spreading calipers).
ASBT	Acetabulosacral buttress thickness	Minimum thickness of the acetabulosacral buttress.
IB	Iliac breadth	Direct distance from the superior limit of the AIIS to the greater sciatic notch.
AD	Acetabular diameter	Distance from the rim of the acetabulum at the ischium to the rim just below the anterior inferior iliac spine.
HMA	Hamstring moment arm	Straight line distance from the center of the acetabulum to the center of a vertical line separating the origin of the <i>M. semimembranosus</i> from that of the combined tendon of <i>Mm. biceps femoris</i> and <i>semitendinosus</i> .
TAS	Tuberoacetabular sulcus width	Minimum distance between the tuberosity and the margin of the acetabulum.

\*For details see Kibii et al. 2011 SOM. All measurements taken with sliding calipers unless otherwise noted.

and PIIS is straight. There is no trace of a posterior gluteal line on the posterior surface (the specimen does not seem to extend far enough superiorly to catch the line), and the attachment area of *M. gluteus maximus* is smooth and featureless. A small, rugose crest at the PIIS marks the attachment of *M. piriformis*.

The greater sciatic notch is relatively wide, but the superior margin is very short in its anteroposterior dimension. Sciatic notch breadth (direct distance from the middle of the PIIS to the posterior ischial margin of the notch, taken perpendicular to the posterior ischial margin) is 17.3mm. The other dimensions of the sciatic notch cannot be estimated as only the iliac portion of the notch is represented (the right ischium is unfused and missing). The portion of the preserved arcuate line is broad and rounded, resembling a pillar. The acetabulosacral buttress is thick (18.5mm

ML at its thickest, roughly midway between the acetabulum and auricular surface). The minimum distance from the joint surface of the acetabulum to the apex of the auricular surface (the acetabulosacral load arm: Table 1) can be estimated at 43.5mm. The preserved portion of the iliac fossa is smooth and featureless.

On the anterior margin of the iliac blade there is a small crest marking the inferior extent of the insertion of *M. sartorius*. The attachment area for the secondary center of ossification at the AIIS is narrow, with a mediolateral dimension of 5.4mm at mid-spine (A.L. 288-1, of comparable body size, has an ML dimension of 8.7mm at mid-spine [as measured on a cast]). The AIIS of MH1 is also markedly curved and relatively short superoinferiorly, measuring 21.1mm. MH1 and the *Au. africanus* specimen StW 431 have similar curvatures to their AIIS, although the spine is much thicker

in the latter (8.1mm ML at mid-spine in StW 431 vs. 5.4mm in MH1). It is also apparent from the preserved morphology that the anterior margin of the iliac blade has a sigmoid curvature to it, as is common in *Homo* (Ward et al. 2015). StW 431 has a very slight sigmoid curvature, while other specimens attributed to *Au. africanus* (Sts 14, MLD 7, and MLD25) have straight anterior borders (as do those of other australopiths: SK 3155b, SK 50, and A.L. 288-1). The distance from the superior-most point of the attachment for the secondary center of ossification for the AIIS to the inferior-most point of the *M. sartorius* origin is very short, measuring approximately 10mm (compare with that of A.L. 288-1, of roughly similar body size, which measures ca. 20mm).

The SI shortness of the AIIS may indicate a relatively reduced attachment area for *M. rectus femoris*. Nonetheless, there is a pronounced lateral projection of the superior region of the acetabular rim, creating a shelf-like projection and an adjacent, distinct sulcus in the attachment area of the fibrous portion of the acetabular labrum and the reflected tendon of *M. rectus femoris*. This has been considered a derived feature of *Homo* (Simpson et al. 2008), although the australopith StW 431 evinces similar morphology. The relative sizes of the two attachment areas may indicate a greater emphasis on the reflected rather than straight head of *M. rectus femoris*. The inferior portion of a distinct iliac pillar arises from the posterior margin of the superior rim of the acetabulum. There is a nutrient foramen slightly anterior to this pillar.

#### U.W. 88-102: Partial Left Ilium

**Preservation.** This specimen represents most of the left ilium, lacking only the anterior superior portion of the iliac blade (including the ASIS) and all of the iliac crest (Figure 3). The fragment has a maximum SI dimension of ca. 105mm, and a maximum AP dimension of ca. 101mm. The entirety of the iliac contribution to the acetabulum is preserved. However, unlike the right-side ilium of MH1, U.W. 88-102 completely lacks any of the lunata surface, indicating that the iliac acetabular epiphysis had not fused to the iliac body on this side at the time of MH1's death. The anterior margin preserves the AIIS, but is broken immediately superior to it. The apophysis of the AIIS appears to have fused on this side (unlike the right side). The anterior margin of the iliac blade is broken through the acetabulocrystal buttress (iliac pillar), just superior of the AIIS. The remainder of the anterior margin of the iliac blade presents as a jagged bone surface with adherent matrix, with some small islands of cortical bone embedded in the matrix. The blade preserves about 46mm (AS-PI) of the iliac fossa, above which is found a short (ca. 15mm) section of broken iliac crest (with adherent matrix both anterior and posterior to this exposed section). While this appears to represent a pre-fossilization fracture just inferior to the iliac crest, it is also possible that it represents a portion of the unfused attachment area for the iliac crest apophysis. Posteriorly, the bone is complete from the unfused growth surface for the ischium inferiorly to the PSIS. The auricular surface is intact, and the iliac tu-

berosity and most (perhaps all) of the postauricular area is preserved. Matrix still adheres to the area of the iliac crest superior of the postauricular area.

Both the internal and external surfaces of the left ilium have multiple prominent cracks through the surficial cortical bone. On the internal surface these present mainly as three parallel vertical cracks (with a slight posteroinferior to anterosuperior direction). All of these cracks have some small degree of matrix infilling that has slightly displaced the adjoining surfaces relative to one another. The most inferior and largest of these cracks begins at the acetabular margin and runs to the broken anterior margin at the top of the iliac pillar. The smaller two cracks run through the iliac fossa. The anterosuperior corner of the preserved portion of the iliac fossa is cracked into roughly ten small fragments of cortical bone, which are held in place by matrix. Damage to the external surface manifests predominately as a single, large, fan-shaped radiating fracture in the anterosuperior half of the iliac blade. The fracture begins as a single vertical crack at the lateral margin of the acetabulum, which travels superiorly about 17mm before radiating into four fractures, ranging in orientation from AS-PI to PS-AI. The constellation of fractures produces three large triangular segments of cortical bone, which are held in place by matrix. The surface of the fractured area is slightly depressed relative to the adjacent gluteal surface. Superior to the fan-shaped fracture area are three relatively large fragments that are held in place by matrix. A smaller, irregular fracture can be seen on the posterior part of the lateral surface, adjacent to the PIIS. Finally, a 21mm (AP) by 16mm (SI) segment of iliac blade is missing, creating a hole through the superoposterior part of the iliac and gluteal fossae.

**Morphology.** Damage to the anterior iliac blade precludes the measurement of blade dimensions. The iliac breadth (superior limit of the AIIS to the sciatic notch: Kibii et al. 2011 SOM) is 53.5mm. The iliac fossa is deeper than seen in adult *Au. africanus* specimens Sts 14 and StW 431, but shallow relative to *Homo sapiens*. Based on the iliac blade adjacent to the (missing) crest, the iliac crest has a posterior angle (at the spina limitans) of about 145° (similar to other australopiths and *Homo*: Kibii et al. 2011 SOM), which produces a moderately deep posterior gluteal fossa. The posterior gluteal line is visible about 10mm anterior of the PSIS: the anterior and inferior gluteal lines cannot be discerned. The iliac pillar is pronounced, running anterosuperiorly from the lateral acetabular margin until it reaches the broken anterior margin of the iliac blade. The lack of the anterior iliac blade makes it impossible to know if the buttress terminated in a distinct crystal tubercle (and was thus an acetabulocrystal buttress) or if it instead ended at the ASIS (in which case it would be an acetabulospinal buttress). The pillar is 7.9mm thick at the break, and has a maximum thickness of 12.3mm near its base (by comparison, the iliac blade is ca. 6mm thick adjacent to the buttress). The pillar is not as strongly developed as it is in some specimens that have been attributed to early *Homo* (such as KNM-ER 3228 [Rose 1984] or OH 28 [Day 1971]), but it is thicker and more well-defined than the in-



Figure 3. Fragmentary left ilium (U.W. 88-102) of MH1 in internal (top row, left), anterior (top row, right), external (middle row, left), posterior (middle row, right), superior (bottom row, left) and inferior (bottom row, right) perspectives (scale bar in centimeters).

distinct thickening of the anterior-most iliac blade seen in other australopiths (A.L. 288-1, Sts 14, MH2, MLD 7, and SK 3155b all have poorly defined and very slight thickened buttresses in the anterior iliac blade; StW 431 and MLD 25 have somewhat more pronounced thickenings, but still not to the extent seen in MH1). In terms of the angle formed between the iliac pillar and a line connecting the AIIS and PIIS, MH1 does not differ from other australopiths (Kibii et al. 2011 SOM). However, the pillar appears to be offset dorsally (that is, more posteriorly positioned relative to the AIIS and ASIS than seen in other australopiths), and this suggests MH1 may have had a true acetabulocrystal buttress rather than the acetabulospinal buttress usually found in

the ilia of australopiths.

Unlike the right-side auricular surface (U.W. 88-7), the left side auricular surface, although still L-shaped, lacks a well-defined upper limb. Close examination of the area subjacent to the anterior part of the iliac tubercle reveals a poorly defined contact area for the left dorsal alar tubercle of the sacrum, although the anterosuperior margin of the auricular surface can be discerned. The lower limb of the auricular surface has a length (apex-PIIS) of 30.0mm and an average height of 12.2mm. The upper limb has a length of 24.2mm and an average width of 11.8mm, for a total auricular area (Kibii et al. 2011 SOM) of 536.7mm<sup>2</sup>. A very slight and short preauricular sulcus can be seen below the auricu-

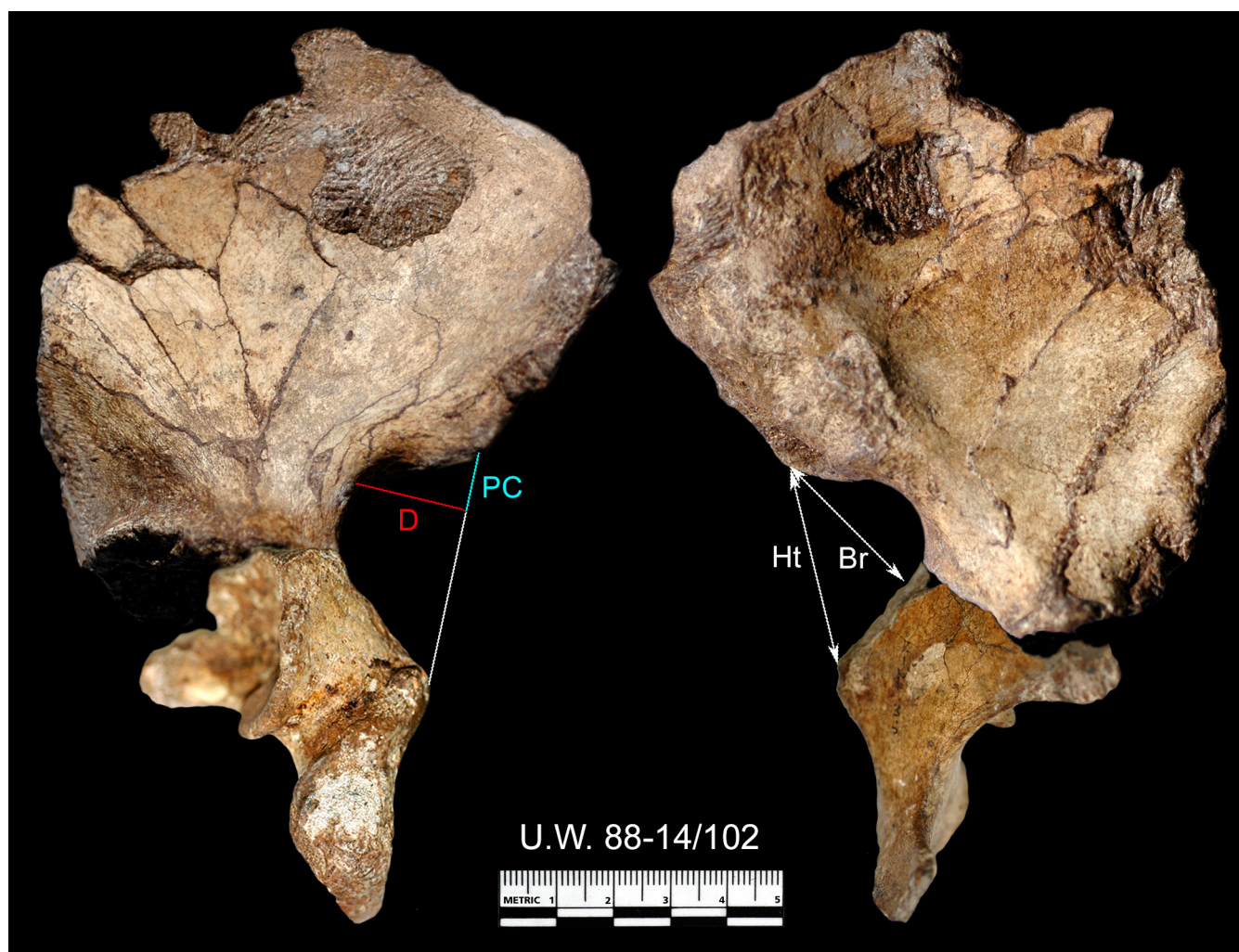


Figure 4. Fragmentary left os coxae of MH1 formed by refitting U.W. 88-102 and U.W. 88-14 in external (left) and internal (right) perspectives. Dimensions of the reconstructed greater sciatic notch (see discussion of morphology of U.W. 88-102) are illustrated as follows: height (Ht); breadth (Br); depth (D, in red); and posterior chord of sciatic notch breadth (PC, in blue) (scale bar in centimeters).

lar surface. As in the right-side fragment, the anterior margin of the auricular surface falls about 5mm anterior of the greater sciatic notch, as is common among modern human males (Arsuaga and Alonso 1983).

The postauricular surface extends roughly 30mm superior of the auricular surface. The iliac tuberosity presents as a single, ill-defined and rugose tubercle traversing most of the width of the postauricular area, to about 30mm anterior of the posterior margin of the ilium. The size and morphology of the iliac tuberosity suggests hypertrophy of the interosseous sacroiliac ligament relative to that seen in the adult australopiths A.L. 288-1 and Sts 14. The posterior margin of the ilium between the PSIS and PIIS is straight, and the posterior margin of the iliac blade at the PSIS is relatively thin (ca. 9mm ML). As with the right ilium, a small, roughened crest at the PIIS marks the attachment of *M. piriformis*.

Refitting of the left iliac blade with the left ischium U.W. 88-14 (described below) provides some information about

the morphology of the greater sciatic notch and allows for a rough estimation of its dimensions (Figure 4). Estimated notch height (direct distance from the middle of the ischial spine to the middle of the PIIS; called breadth by many researchers, e.g., Bruzek 2002) is 48mm, while the breadth (direct distance from the middle of the PIIS to the posterior ischial margin of the notch, taken perpendicular to the posterior ischial margin: measurement M 15.1 in Bräuer 1988) is 37mm. The estimated notch depth (Bruzek 2002; Simpson et al. 2008) is 19.5mm, while the point of deepest inflection of the notch (Simpson et al. 2008; also called the posterior chord of sciatic notch breadth: Bruzek 2002) falls 13.8mm inferior of the PIIS, producing an inflection index (see Simpson et al. 2008) of 0.29. This index value falls in the area of overlap between modern human males and females (Simpson et al. 2008), however, the appropriateness of this measure as a discriminator of sex in fossil hominins has not been established.

There is some slight rugosity on the preauricular sur-

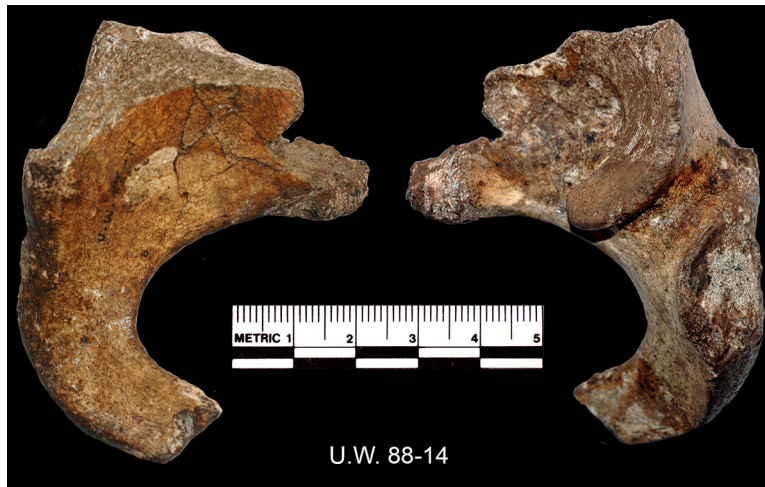


Figure 5. Left ischium (U.W. 88-14) of MH1 in internal (left) and external (right) perspectives (scale bar in centimeters).

face (adjacent to the greater sciatic notch and inferior to the auricular surface) in the area of the superior-most line of attachment of *M. obturator internus*. The portion of the preserved arcuate line is broad and rounded, although somewhat sharper and more distinct than in the right side. The acetabulosacral buttress is thick (maximum thickness of 18.6mm ML, midway between the acetabulum and auricular surface). A reasonable estimate of acetabulosacral load arm (minimum distance from auricular apex to lunate surface) can be made by aligning the right-side fragment U.W. 88-6, on which the acetabular epiphysis with the lunate surface has fused, with the less-developed acetabulum of U.W. 88-102. This produces a load arm estimate of ca. 43mm.

The mediolateral dimension of AIIIS at mid-spine is 5.8mm, and is thus narrow like the right side (5.4mm), as compared to australopiths such as A.L. 288-1 (8.7mm) and StW 431 (8.1mm). Like the right-side AIIIS, it is markedly curved (medially deflected) and relatively SI short (23.1mm), although slightly longer than its antimeres (21.1mm). In all other aspects of morphology, the left-side AIIIS spine is like that of the right (see above).

As with the right-side ilium, there appears to be a pronounced lateral projection of the superior region of the acetabular rim. The rim of the acetabulum is not as well developed in the left ilium as it is in the right, and thus the shelf-like projection and adjacent sulcus are not as well formed. Even still, the preserved epiphyseal margin is projecting and a sulcus is evident, suggesting that with fusion of the acetabular epiphysis the morphology on the left would match that on the right.

#### U.W. 88-14: Left Ischium

**Preservation.** This largely complete ischium preserves the ischial contribution to the acetabulum, the body, the ischial tuberosity (lacking the unfused apophysis) and the ramus (Figure 5). The maximum AP dimension of the fragment is approximately 52mm, while the SI height is approximately 69mm. The bone has only two fracture surfaces—ventrally the ramus is broken at about the point of transition to the

inferior pubic ramus; dorsally the ischium is ‘planed off’ through the ilioischial eminence immediately dorsal to the acetabulum and at the same craniocaudal level as the iliopubic eminence. This latter fracture plane is oriented from superolateral to inferomedial, and extends down to and through the ischial spine, thus creating the loss of the superodorsal portion of the ischium. The fracture exposes trabeculae over its entire surface; while the fracture does not appear fresh (the surface is of the same color as the neighboring subperiosteal bone), neither does it appear to have happened prior to fossilization (there is no matrix embedded in the trabeculae), and thus it is likely to represent blasting damage by miners. Overall the surface preservation is good, although there are some small areas of cortical exfoliation on the ischial ramus. A very fine crack encircles the ischial ramus at the inferoposterior corner of the obturator foramen and completely separates the ischial ramus from the body, although the pieces remain firmly connected to one another. Other small superficial cracks also are evident on the ventral surface of the ischial body.

The ischium had not fused to the pubis or the ilium at the time of death of MH1. A portion of the epiphyseal contact with the ilium at the superodorsal corner of the acetabulum is preserved, as is the epiphyseal contact with the os acetabulum (the ossified remnant of the triradiate cartilage: Ponseti 1978) at the anteroinferior corner of the acetabular notch. While it appears that the os acetabulum is missing, it is possible that a small bit of its most inferior portion is adhering to the ischium. The ischial contribution to the lunate surface develops from its own secondary center of ossification (Ponseti 1978), and in U.W. 88-14 this acetabular epiphysis was fully fused to the body of the ischium. The secondary center of ossification for the ischial tuberosity is unfused and missing.

**Morphology.** The estimated ischial length (mid-acetabular point on the superior margin of the acetabular notch to the furthest point on the ischial tuberosity) is 64mm (adding one millimeter for the missing apophyseal surface of the ischial tuberosity). The preserved portion of the acetabular

rim is well-formed. At its widest point, the lunate surface measures 16mm (AM-PL). The anteroinferior end of the lunate surface forms a projecting lip, creating a deep sulcus in the dorsal edge of the acetabular notch. The acetabular notch measures 16.8mm AP. The tubercle to which the anterior end of the transverse ligament attaches is preserved as a rugose crest. The acetabular fossa is wide and shallow.

The superolateral margin of the obturator foramen is thin and rounded, and is similar to the morphology seen in A.L. 288-1 and Sts 14. The analogous margin tends to be relatively thicker in modern humans but exhibits a sharper crest in chimpanzees (although the extent to which this trait is affected by body size and/or the subadult status of MH1 is unclear). The superoinferior dimension of the obturator foramen is a minimum of 34.5mm. No posterior obturator tubercle (for the superior ligamentous band of the obturator membrane) is visible, and the obturator groove is indistinct.

The apophyseal surface for the ischial tuberosity is crescent-shaped with a marked lateral eversion. The superior portion of the tuberosity (the attachment surface for the hamstring muscles) faces laterally, resembling the morphology seen in some specimens that have been attributed to early *Homo* (such as OH 28: Day 1971; KNM-ER 3228: Rose 1984; and other archaic *Homo*: Stringer 1986). While it is sometimes said that apes also have laterally facing ischial tuberosities (Aiello and Dean 1990), it is more the case that they tend to have posterolaterally facing tuberosities (Robinson 1972) with an expansion of the superolateral portion, which is a morphology distinct from the laterally rotated tuberosities in some specimens attributed to early *Homo*. This morphology appears to be variable in specimens attributed to early *Homo*, as at least one fossil (the 1.07-0.99 Ma ischium UA 405 from Buia, Eritrea: Hammond et al. 2018) exhibits a more medially oriented ischial tuberosity. In MH1 the superior face of the tuberosity possesses a flange-like ventral projection at its widest part, which forms a distinct crest at its juncture with the ventrolateral surface of the ischial body. Moving superiorly, the apophyseal surface for the tuberosity curves medially towards where the ischial spine and lesser sciatic notch would be. The projecting rim of the tuberosity along its superior and medial margins, in concert with the projecting rim of the acetabulum, forms a deep and narrow tuberoacetabular sulcus for the *M. obturator internus*. Inferiorly, the attachment area for *M. adductor magnus* lies at an angle of about 125° to the superior face. The apophyseal surface of the tuberosity continues along the ischial ramus ventrally until it is interrupted by the break in the ramus. The maximum breadth of the tuberosity (minus the secondary center of ossification) is 18.2mm. The width of the tuberoacetabular sulcus (the minimum distance between the tuberosity and the margin of the acetabulum) is 9.5mm, which suggests a relatively short ischium as exemplified by early *Homo* and modern humans rather than other australopiths and chimpanzees (Kibii et al. 2011 SOM; Lovejoy et al. 2016).



Figure 6. Left pubis (U.W. 88-68) of MH1 in internal (left) and external (right) perspectives (scale bar in centimeters).

#### U.W. 88-68: Left Pubic Symphysis

**Preservation.** This specimen preserves the partial body and symphysis of the left pubis (Figure 6). There is an oblique (superolateral to inferomedial) break through the body, and the fracture is occluded with matrix. The symphyseal face has also been planned off (obliquely, from dorsomedial to ventrolateral), and matrix has infilled the trabecular bone deep to the symphysis. Nonetheless, a few small spots of the original epiphyseal surface can be made out along the dorsal margin of the symphysis. About 25mm of the medial portion of the superior pubic ramus remains, although the superior margin is abraded.

**Morphology.** Little can be said about the morphology of the MH1 pubis from this fragment. The pubic tubercle is either absent due to damage, or was not well developed. The symphysis, judging from the preserved portion of the medial pubic body, was roughly 34.5mm superoventral-inferodorsally by ca. 10mm superodorsal-inferoventrally.

#### OSSA COXAE OF MALAPA HOMININ 2 (MH2)

##### U.W. 88-52/133/136: Partial Right Os Coxae

**Preservation.** Three fragments conjoin to produce a largely complete right ilium and a complete right pubis. U.W. 88-133 (Figure 7) is a nearly complete iliac blade and body, while U.W. 88-52 is a mostly complete pubis (Figure 8). U.W. 88-136 is a small fragment of superior pubic ramus that joins U.W. 88-133 with U.W. 88-52 (note: U.W. 88-136 was initially designated U.W. 88-52B in Kibii et al. 2011, but was later given its own catalog number).

The ilium is missing the anterior portion of the blade, with a fracture surface extending from the anterior iliac crest in the region of the cristal tubercle (note: it is likely that MH2 did not possess a cristal tubercle [see below], such that it might be more accurate to say the point of anterior inflection of the curvature of the iliac crest) to the AIIS. The ASIS is thus missing. Most of the iliac fossa is preserved,



Figure 7: Right ilium (U.W. 88-133) of MH2 in internal (top row, left), anterior (top row, right), external (middle row, left), posterior (middle row, right), superior (bottom row, left) and inferior (bottom row, right) perspectives (scale bar in centimeters).

as is the entirety of the gluteal fossa externally and auricular surface plus the postauricular area internally. The ilium preserves the superior half of the acetabulum and most of the lunate surface, as well as the superior portion of the acetabular fossa with the ligamentum teres attachment site. Posteroinferiorly the fragment preserves a small portion of the ischial contribution to the acetabulum, but does not include the ischial spine nor ischial tuberosity. Anteroinferiorly the fragment ends at the base of the superior pubic ramus.

A small notch of bone, 4.9mm wide, is missing from the iliac crest about midway between the spina limitans and the region of the cristal tubercle (but see below). Numerous small cracks can be seen on both the medial (internal) and lateral (external) surfaces of the bone, and the external surface appears mildly weathered and pitted. There is a small (ca. 3.5 x 2mm) hole through the iliac blade in the middle of the gluteal fossa.

While the numerous fine cracks on the surface of the iliac blade appear to have no appreciable effect on the



Figure 8. Right pubis (U.W. 88-52) of MH2 in internal (right), medial (center) and external (left) perspectives (scale bar in centimeters).

shape of the bone, two larger cracks have created a small amount of distortion to the fossil. One of these cracks is evident on the exterior surface, beginning at the iliac crest about 30mm anterior of the posterior superior iliac spine (PSIS). This crack extends inferiorly, becoming somewhat larger adjacent to the sciatic notch, extending down into the iliac body and through the acetabulum. Just superior of the sciatic notch there is a small (ca. 12.5mm SI) area with displacement of the external bone surfaces, such that the surface posterior of the crack sits about 1.5mm higher than the surface anterior of the crack. There appears to be some displacement of the anterior and posterior parts of the acetabulum relative to one another, creating a small amount of compression of the acetabulum. This can be appreciated by noting that the right femoral head of MH2 fits snugly in the acetabulum, allowing insufficient room for the articular hyaline cartilage that would have covered the two joint surfaces during life. The second distortion-producing crack occurs on the internal surface, beginning adjacent to the AIIS and extending inferiorly onto the base of the superior pubic ramus. At its superior end the crack is 3mm wide, tapering to a hairline fracture as it progresses inferiorly. The surface of the iliac body inferior and lateral of the crack appears to be rotated slightly inferolaterally, which along with the first crack has contributed to the distortion and reduction in size of the acetabulum.

Superior to the anterior acetabular rim, and just postero-inferior to the AIIS, there is a 9.5mm x 2.3mm crevice in the bone, perhaps representing an antemortem lesion. The crevice is hollow, has rounded margins, and has calcite crystals inside of it.

Two fragments of the pubis are preserved. U.W. 88-136 (formerly U.W. 88-52B) is a 24.7mm-long (maximum) fragment that represents the iliopubic eminence and a small

amount of the anterior horn of the acetabulum. The proximal break lies in the transverse plane, and contacts the broken edge of U.W. 88-133 along 12.1mm of its 19.6mm width. The distal break is slanted from superolaterally to inferomedially, such that 19.4mm of the lateral side and 22.4mm of the medial side of the ramus is preserved. The ramus measures 12.7mm SL-IM at the break. There is a shallow fracture ca. 3mm wide along the anteromedial surface of the fragment, which aligns with the fractures on U.W. 88-133 and U.W. 88-52. U.W. 88-136 refits cleanly with the pubic fragment U.W. 88-52, but lacks a tightly articulating surface with U.W. 88-133. The conjoining surfaces of U.W. 88-136 and U.W. 88-133 refit well along the lateral part of the break (but do not form a clean contact), and the keystone piece preserves the superoanterior corner of the acetabulum, which allows for the confident reassembly of the iliopubic ramus (Figure 9: see also Kibii et al. 2011).

U.W. 88-52 retains most of the superior pubic ramus, the pubic symphysis, and the inferior pubic ramus. The break on the superior ramus is slanted superolaterally to inferomedially (matching the break in U.W. 88-136, with which it refits cleanly), preserving 56.4mm of the lateral side of the ramus, and 52mm of the medial side of the ramus (measured from the symphysis). A shallow fracture, ca. 2mm wide, is present along the anteromedial edge of the proximal end of the superior pubic ramus. The fracture extends about 16mm distally and is continuous with the fracture across the anteromedial surface of U.W. 88-136.

The preservation of U.W. 88-52 is excellent. Two small cracks can be seen on the inferior pubic ramus: a very faint crack encircles the ramus at its juncture with the pubic body, and a somewhat more substantial crack encircles the ramus about 30mm from the inferior-most point of the symphyseal surface. Neither crack shows evidence of dis-

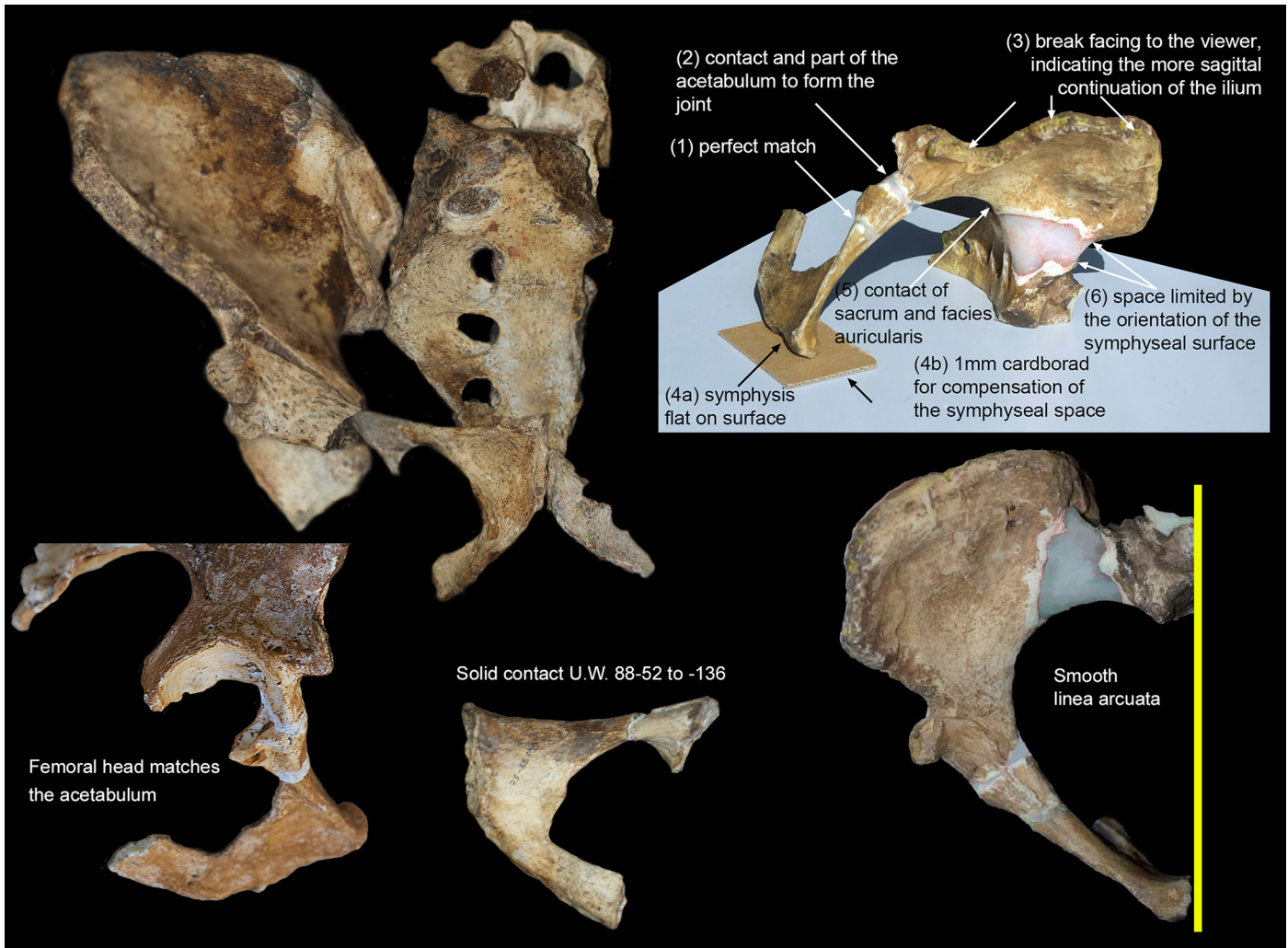


Figure 9. Details of the reconstruction of the MH2 partial pelvis, as employed by Kibii et al. (2011).

tortion. The rest of the fragment is in excellent condition.

**Morphology.** The ilium is 93.8mm high, from the mid-acetabular point on the superior margin of the acetabular notch to the most distant point on the iliac crest. The iliac blade itself is 84.2mm high, measured from the arcuate line (midway between the iliopubic juncture and the anterior end of the auricular surface) to the most distant point on the crest (reconstruction of the missing anterior iliac crest and ASIS [Kibii et al. 2011] suggests that this dimension would not change if the blade were intact). The superior breadth of the blade cannot be measured; the inferior breadth, from the AIIS to the PIIS, is 88.8mm (this dimension, however, is affected by a few millimeters of exostotic outgrowth at the AIIS: see DeSilva et al. 2013). Iliac breadth (superior limit of the AIIS to the greater sciatic notch: Kibii et al. 2011 SOM) is 50.5mm.

Interiorly, there is a moderately deep iliac fossa, and a large attachment site for the *M. iliacus*. There is a distinct sigmoid curvature of the iliac crest—although the anterior portion of the blade is missing, the anterior-most preserved portion of the blade is curving medially, indicating a medially displaced ASIS. The iliac crest has a posterior angle (at

the spina limitans: Table 1) of  $136^\circ$  and an anterior angle (in the region of the cristal tubercle: see Table 1) of  $155^\circ$ . Exteriorly, the inferior and anterior gluteal lines are not evident. The posterior gluteal line presents as a distinct ridge about 11mm anterior of the posterior margin of the ilium. The gluteal fossa is deep, attaining a maximum depth of about 14mm. The superolateral edge of the anterior crest is everted laterally, and there is a small amount of exostotic lipping of the bone on the exterior surface of the crest at the attachment for the external abdominal oblique muscle. The adjacent surface for the *M. transversus abdominis* is featureless. Moving posteriorly, the crest remains relatively thin (5–6mm) from the anterior break to the posterior end of the *M. quadratus lumborum* attachment (at the spina limitans), where it widens to about 7mm. The crest narrows again (to about 5mm) before widening (to 12mm) in the area of the *M. latissimus dorsi* attachment leading to the PSIS. On the interior surface of the posterior ilium there is a clear demarcation between the attachment area for the erector spinae muscle and the iliac tuberosity for the posterior sacroiliac ligament. The area of origination for *M. erector spinae* is quite large, measuring 13.9mm SI at the level of the an-

terior end of the auricular surface and 20.3mm at the PSIS.

The area of the cristal tubercle is missing from the anterosuperior portion of the blade. The anterior iliac blade evinces no clear acetabulocristal buttress (iliac pillar), although some thickening of the anterior base of the blade (just superior of the AIIS) suggests that MH2 might have had an indistinct and anteriorly positioned iliac pillar as in other australopiths (such as A.L. 288-1, Sts 14, StW 431, SK 3155b, and the juvenile specimens MLD 7 and MLD 25). Damage to the anterior iliac blade and loss of the ASIS precludes the assessment of whether the buttress terminated at the ASIS (that is, an acetabulospinous buttress) as in some australopiths (such as Sts 14 and StW 431), or whether it terminated on the iliac crest at a distinct cristal tubercle (that is, an acetabulocristal buttress) as in most specimens of *Homo*.

The auricular surface is L-shaped, with an upper extremity that is 25.7mm long and has an average width of 7.7mm. The lower extremity has a length (apex-PIIS) of 33.7mm and an average height of 12.2mm, for a total auricular area (Kibii et al. 2011 SOM) of 515.1mm<sup>2</sup>. There is a distinct preauricular sulcus, which is accentuated by a crest-like tubercle for the *M. piriformis* laterally. When the ilium is held in anatomical position, the anterior corner of the auricular surface lies ca. 4mm posterior of the greater sciatic notch. This feature is sexually dimorphic in living humans, with the posteriorly positioned auricular surfaces (as in MH2) being characteristic of females (Arsuaga and Alonso 1983).

Posteriorly, the ilium is robust. A postauricular groove (at the insertion of the posterior interosseous ligament) is small, but noticeable. The retroauricular area is posteriorly expanded, and contains a large iliac tubercle which presents as one large tubercle (lying about 16mm above the superior margin of the posterior part of the auricular surface, and about 9mm anterior of the posterior margin of the ilium) and two smaller tubercles—one 8.5mm inferior and one 15.7mm anterior of the large tubercle. There is also what appears to be an osteophyte on the anterior margin of the retroauricular area, about 35mm anterior of the PSIS and 24mm inferior of the iliac crest. The PSIS is robust, and contributes to a large attachment site for the erector spinae muscle. The PIIS is prominent and projects posteriorly about 5mm beyond the posterior margin as a result of a bony outgrowth on the spine.

The greater sciatic notch is wide. Because the ischial spine is missing, a direct measure of the height of the notch (direct distance from the middle of the ischial spine to the middle of the PIIS. Also known as sciatic notch breadth, e.g., Bruzek 2002) cannot be obtained. A minimum height can be had by measuring to the most inferior point on the preserved posterior border of the ischium, which produces a value of 43.2mm. In modern humans the ischial spine generally falls on a line directly inferior of the PIIS when the os coxae is held in anatomical position—if the position of the ischial spine of MH2 is reconstructed in this way (by extending the line of the posterior ischial border until it intersects a vertical dropped from the PIIS) the estimated

notch breadth is 47mm. Sciatic notch height (direct distance from the middle of the PIIS to the posterior ischial margin of the notch, taken perpendicular to the posterior ischial margin) is 40.3mm. Again, using a reconstructed position of the ischial spine, the estimated notch depth (Bruzek 2002; Simpson et al. 2008) is 24.3mm and the estimated point of deepest inflection of the notch (Simpson et al. 2008; also called the posterior chord of sciatic notch breadth: Bruzek 2002) is 27mm inferior of the PIIS. This produces an inflection index (see Simpson et al. 2008) of 0.57. This value falls above the range of variation in a small sample of modern humans, and thus MH2, like the taxonomically uncertain BSN 49/P27 specimen, has a sciatic notch morphology that is “hyperfemale” (Simpson et al. 2008: note however that the utility of this measure as a discriminator of sex in fossil hominins has not been established).

The arcuate line is broad and rounded in MH2. There is a well-developed acetabulosacral buttress, attaining a thickness of 17.2mm midway between the acetabulum and auricular surface. The shortest distance between the acetabular joint surface and the apex of the auricular surface (the acetabulosacral load arm: Kibii et al. 2011 SOM) is 37mm.

The anterior border is long, with a large distance between the AIIS and the approximate position of the ASIS. The superior surface of the AIIS is broken, but the inferior portion of the spine is anteriorly projecting, with what appears to be an osteophytic lip of bone projecting from the inferolateral portion of the spine. Osteophytic hypertrophy of the AIIS suggests large habitual strain at the origins of the *M. rectus femoris* or the attachment of the iliofemoral ligament (DeSilva et al. 2013).

Unlike the ilia of MH1, the ilium of MH2 does not have a shelf-like attachment for the reflected head of *M. rectus femoris*. There is, however, a very shallow sulcus laterally adjacent to the AIIS, which is similar to the morphology (although the sulcus is not as distinct or deep) seen in StW 431 and SK 3155b.

The acetabulum is very slightly distorted and is incomplete. The maximum breadth across the preserved portion of the acetabulum (taken anteroposteriorly) is 34mm, although the actual dimension would have been greater. The acetabulum attains a maximum depth (from the level of the lateral rim to the deepest point in the acetabular fossa) of 16.7mm. The cotylosciatic breadth (the minimum distance from the acetabular rim to the greater sciatic notch: İşcan and Steyn 2013) is 23.6mm. The lunate surface attains a maximum breadth of 16.9mm at the superior-most part of the acetabulum. The lunate surface is continuous across the entire preserved portion of the acetabulum, and continues anteroinferiorly well past (by about 15mm) the position of the AIIS.

The pubis is fairly long (pubic length=81.8mm, from the mid-acetabular point on the superior margin of the acetabular notch to the most medial point on the middle of the superior symphyseal surface, based on the reconstruction of Kibii et al. 2011), and presents a wide pubic body (measuring 26.9mm PS-AI at the level of the inferoanterior corner of the obturator foramen and 33.4mm PS-AI at



Figure 10. Fragmentary left pubis (U.W. 88-10) of MH2 in internal (left), medial (center) and external (right) perspectives (scale bar in centimeters).

the superoanterior corner of the obturator foramen). The obturator groove (sulcus) is very weakly developed. The pubic tubercle (for the inguinal ligament) is located on the superomedial corner of the external surface of the pubic body, as also seen in A.L. 288-1 (Simpson et al. 2008) but not in living humans. The pectineal line begins as a broad rounded ridge at the acetabulum that develops into a distinct rounded crest as it moves towards the pubic tubercle. This crest is interrupted by an area (roughly 15mm long) of mild rugosity ending about 8mm lateral of the pubic tubercle, which appears to indicate the medial extent of *M. pectineus*. The anterior surface of the pubic body is smooth and presents a slight concavity in the region of the *M. adductor longus* origin. The internal (posterior) surface has a mild concavity in the mediolateral direction, and the dorsal margin of the symphyseal surface is rugose and presents one and possibly two areas of cortical resorption (pitting, or “scars of parturition”: Maass and Friedling 2016; Stewart 1970).

The symphyseal face is long and narrow, with a height of 34.3mm and an average breadth of 10.9mm (minimum: 9.9mm; maximum 13.1mm). The symphyseal face is an irregular rectangle in shape. The symphyseal surface is fairly smooth: there is no billowing on the face, although there are the remnants of two ridges on the inferior half of the symphysis. There is a nearly complete ridge outlining the symphyseal face, with only the ventrosuperior ridge incomplete. This morphology corresponds with Phase 4 of the Suchey-Brooks pubic symphysis scoring method (Brooks and Suchey 1990). Anterior to the symphyseal surface there is a considerable area of nonarticular bone, forming a sulcus-like depression that is 17.4mm long (anteroposteriorly) by 6.8mm (superoinferiorly) at its widest point.

The inferior pubic ramus is relatively featureless on its anterior surface, although there is a low rounded ridge on its inferior margin in the area of the *M. gracilis* origination. The inferior margin is rough and slightly everted. Internally, there is some slight rugosity to the inferior margin of the

obturator foramen in the area of the *M. obturator internus* attachment.

#### U.W. 88-10: Left Pubic Fragment

**Preservation.** This fragmentary pubic bone preserves most of the left inferior pubic ramus and roughly half of the pubic symphysis (the inferoposterior half) (Figure 10). The body of the pubis is not preserved. The fragment has a maximum length of 58.3mm. The break in the inferior ramus is irregular and slants from superoanterior to inferoposterior. The break through the symphysis runs from anterosuperior to posteroinferior.

**Morphology.** The overall morphology is similar to that of the right pubis U.W. 88-52. Like the right pubis, the U.W. 88-10 pubic symphysis has a distinct ridge around the symphyseal surface, which demarks a nonarticular sulcus on the anterior side of the symphyseal face. The inferior margin of the ischiopubic ramus is rugose as in its antimer, but differs in having little to no eversion. No pitting is evident on the inferior dorsal symphyseal margin.

## SACRA

### SACRUM OF MALAPA HOMININ 2 (MH2)

#### U.W. 88-137/127: Partial Sacrum

**Preservation.** The partial sacrum U.W. 88-137 preserves almost all of the sacral bodies intact (except for that of the S1, although much of the missing portion of the S1 is preserved, attached by matrix to the centrum of the ultimate lumbar vertebra U.W. 88-126; this detached segment of sacral body is designated U.W. 88-127), as well as the inferior half of the ala on the right side (Figure 11). The specimen is cranio-caudally complete along the midline (except for the detached portion of the S1 body), preserving the entire median crest dorsally. All four of the right-side sacral foramina are intact both ventrally and dorsally. The sacrum is incomplete mediolaterally. The left ala is completely ab-

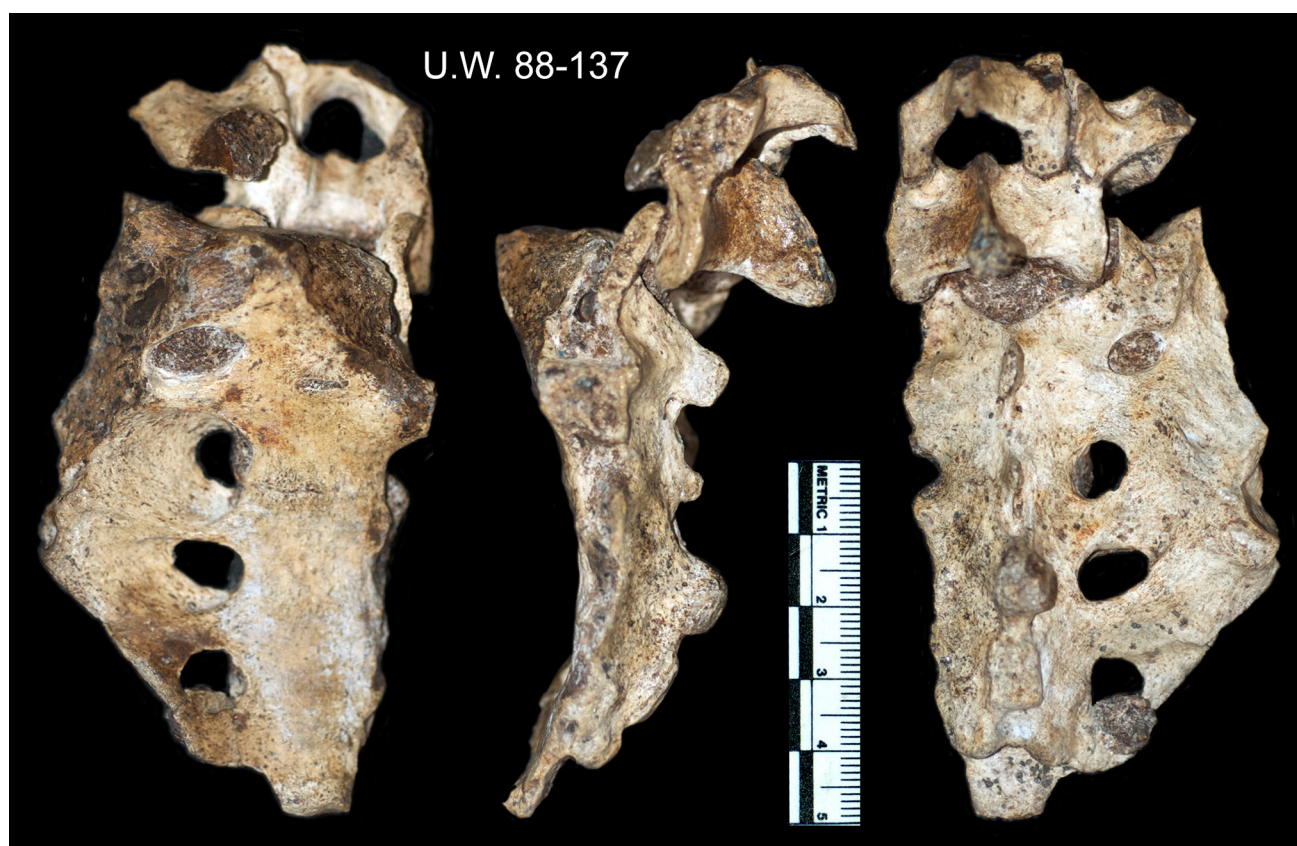


Figure 11. Partial sacrum (U.W. 88-137) of MH2 in anterior (left), lateral (middle) and posterior (right) perspectives (scale bar in centimeters).

sent, preserving only the medial margins of the second, third, and fourth sacral foramina on their respective sacral bodies. The right ala is more complete, yet still not intact: the superolateral portion of the right ala is missing, as is all but the inferior-most corner of the right auricular surface. Superiorly the specimen preserves the right side of the S1 body and the complete right superior articular facet, as well as about one third (ca. 4.5mm) of the left superior articular facet. Portions of the dorsal structures of the ultimate and penultimate lumbar vertebrae are attached to the sacrum by adherent matrix (these vertebrae are described in Williams et al. 2018). These portions include the inferior and superior zygapophyses, laminae, spinous process, right pedicle, and part of the right transverse process of the ultimate lumbar vertebra (U.W. 88-138), and the inferior zygapophyses, partial laminae, and partial spinous process of the penultimate lumbar vertebra (U.W. 88-153). The neural canal formed by the posterior margin of the S1 body and the anterior surface of the last lumbar vertebra is occluded with matrix.

The damage to the left side of the bone occurs about 10–13mm lateral to the median crest. The superior aspect of the left side of the sacral body is broken on a diagonal plane, superomedially to inferolaterally, through the first sacral vertebra. This fracture plane also lies about 45° to the sagittal plane, such that more of the posterior than anterior portion of the sacral plateau is preserved. Anteriorly, roughly 12.5mm of the sacral plateau is preserved (ML);

posteriorly, about 18.9mm of the plateau is preserved (ML). The plane of the fracture surface through the first sacral body lies parallel to the fracture plane through the pedicle of the last lumbar vertebra, and both surfaces are flat, soiled stained, and preserve exposed trabeculae. Both of these fractures thus appear to be the result of miner's blasting. The detached, wedge-shaped portion of the S1 (U.W. 88-127, affixed by matrix to the ultimate vertebra U.W. 88-126) measures 18.2mm ML and 16.1mm AP at its base, and has a SI height of about 13.2mm.

The right ala is broken approximately 31mm from the median crest, and the largely vertical fracture plane (lying in a parasagittal plane, with a slight posterolateral to anteromedial orientation) extends caudally through the lateral (costal) process of the second sacral vertebra. The auricular surface of the third sacral vertebra is preserved, measuring 11.6mm superoinferiorly. The right first sacral foramen is occluded with matrix, and a small nodule of matrix (ca. 9mm in diameter) still adheres to the posterior surface of the lateral process of the fifth sacral vertebra. The lateral process of the fifth sacral vertebra also has a number of fine cracks through it, although the bone appears to be undistorted. There is also a very fine crack on the superior portion of the sacrum, beginning in the depression between the right articular facet and the ala, continuing anteromedially over the anterolateral portion of the superior sacral body, and onto the anterior surface. The crack terminates

in the first right sacral foramen. No distortion is apparent.

**Morphology.** Five distinct sacral bodies are recognizable, with distinct transverse lines separating S1 from S2, and S2 from S3. The sacrum has a ventral height (M-2: M-#s refer to measurements defined in Martin 1928) of 80.2mm, and a dorsal height (M-3) of 82.2mm. The anterior surface is concave, with an estimated ventral arc height of 83mm and a depth (M-6) of 11.7mm; the deepest point is located 35mm superior to the inferior edge of the S5. The posterior surface is correspondingly convex. The specimen has a dorsoventral thickness at the middle of the S2 of 17.6mm, and is thus anteroposteriorly thicker than the sacra of A.L. 288-1 (15.5mm: measured from cast) and Sts 14 (15.2mm), but is not as thick as that of StW 431 (19mm). The ventral sacral body heights are as follows—S1=20.7mm, S2=17.1mm, S3=15.9mm, S4=16mm, and S5=12.6mm. As in modern humans and StW 431 (but not A.L. 288-1 or Sts 14), the auricular surface extends onto the third sacral vertebra.

The dimensions of the sacral plateau can be estimated from the preserved portion of the S1 base. The dorsoventral diameter of the S1 base (M-18) can be estimated at ca. 17mm by reference to the preserved lateral portion of the sacral promontory. The transverse diameter of the body of the S1 (M-19) can be estimated with greater precision, since the dorsal portion of the sacral plateau is preserved past the midline of the bone (thus allowing measurement of the transverse diameter of half of the body). The transverse diameter is thus estimated at 32mm. This produces an estimated first sacral centrum area (square root of the product of the DV and transverse diameters of the sacral plateau: Dobson 2005) of 23.3mm, which is large relative to that of Sts 14 (21.5mm) but small relative to that of A.L. 288-1 (25.2mm), StW 431 (27.1mm) (Dobson 2005), and KSD-VP-1/1 (ca. 31.5) (see Haile-Selassie et al. 2010).

The superior articular facets are paracorally oriented, sitting at an angle of about 50° to the sagittal plane. The complete right facet is gently curved. Although the left facet is damaged, some asymmetry in facet morphology can be made out, as the left side facet projects about 4mm more superiorly than does the right side.

Although the alae are incomplete, reconstruction of the MH2 pelvis (for details see Kibii et al. 2011 SOM) suggests that the alae were mediolaterally broad relative to the size of the S1 body. The form of the auricular surface of the MH2 os coxae (U.W. 88-133) suggests that the sacrum had well-developed dorsal alar tubercles (upper lateral angles), similar to those of the *Au. africanus* specimens Sts 14 and StW 431, but unlike the condition seen in the *Au. afarensis* sacra of A.L. 288-1 (Simpson et al. 2008) or KSD-VP-1/1 (Haile-Selassie et al. 2010).

The first and second spinous processes on the median crest are small, clear and separate, whereas the third and fourth processes are larger and bulbous, and although slightly more fused together than the first and second, remain distinguishable as separate processes. The dorsal sacral intermediate fossa (for the sacroiliac ligaments) is small and the attachment area for the inferior portion of the posterior sacroiliac ligament is nonrugose. The inferi-

or margin of the lateral sacral ridge is nonrugose and not prominent.

Although the MH2 sacrum has a sacral angle (Abitbol 1987) similar to that of A.L. 288-1 (16° in MH2; 15° in A.L. 288-1), the MH2 sacrum exhibits greater curvature of the S3, S4, and S5 bodies, such that its overall curvature is greater than that of A.L. 288-1 (Williams et al. 2013). The dimensions of the superior sacral canal (at the level of S1) cannot be obtained because of obstruction by matrix. Inferiorly, the sacral canal opens at the level of the S5. The laminae of the S5 meet at midline and form a roof over the sacral canal, thus there is not a true sacral hiatus. The canal has a transverse diameter of 12.2mm and a DV diameter of 3.3mm at its terminus.

## COMPARATIVE MORPHOLOGY

### MATERIALS AND METHODS

Comparative data were collected on pelvic remains representing other australopith species, early *Homo* (early to late Pleistocene), and recent *H. sapiens*. Fossil and recent human comparative data were pooled into three groups:

- Australopiths: *Au. afarensis*: AL 288-1 (data from Johanson et al. 1982 and casts), KSD-VP-1/1 (data from Haile-Selassie et al. 2010 and Lovejoy et al. 2016); *Au. africanus*: Sts 14, Sts 65, and StW 431 (all observations on original fossils). MLD 7, MLD 8, and MLD 25 (anthroposcopic observations on original fossils) enter into some of the discussion below, but these juvenile specimens were not entered into any metric analysis; *Au. robustus*: SK 50, SK 3155b, and TM 1605 (all observations on original fossils) and DNH 43 (data from Gommery et al. 2002).
- Early *Homo*: African early Pleistocene *H. erectus* and/or *H. sp. indet.* KNM-ER 3228 (data from Rose 1984 and cast), OH 28 (data from cast), KNM-WT 15000 (observation of original fossils, and data from Walker and Leakey 1993 and Walker and Ruff 1993), BSN 49/P27 (data from Simpson et al. 2008), and KNM-ER 5881c (data from Ward et al. 2015); middle Pleistocene *H. erectus* and/or *H. heidelbergensis*: Arago XLIV (data from cast), Kabwe E719 (data from cast), Kabwe E720 (data from cast), Sima de los Huesos Pelvis 1 (data from Arsuaga et al. 1999); *H. neanderthalensis*: Kebara 2 (data from cast), Krapina 207 (data from cast).
- Modern *Homo sapiens*: South African Nguni skeletons (52 male, 54 female) from the Raymond Dart Collection of the School of Anatomical Sciences, University of the Witwatersrand (all observations on original skeletons). This sample was augmented by 31 individuals from a mixed-sex, mixed-ancestry sample from the collections of the Department of Evolutionary Anthropology, Duke University (see Kibii et al. 2011 SOM).

Measurements are defined in Table 1. Unless otherwise noted, between group differences in median values were evaluated using the Kruskal-Wallis one-way analysis of variance (with  $df=3$  for all tests). This nonparametric test was chosen because small fossil sample sizes precluded the reliable assessment of distributional normality in the data

**TABLE 2. MEAN (SD, N) POSTERIOR (ICPA: at spina limitans) AND ANTERIOR (ICAA: cristal tubercle or most lateral point on iliac crest) ILIAC ANGLES IN AUSTRALOPITHECUS SEDIBA AND COMPARATIVE GROUPS.**

	ICPA <sup>1</sup>	ICAA <sup>2</sup>
<i>Au. sediba</i>	136.3° (1)	154.7° (1)
australopiths	148.2° (9.7°, 2)	169.5° (2.9°, 2)
early <i>Homo</i>	151.8° (14.4°, 4)	141.3° (24.2°, 4)
<i>H. sapiens</i>	145.7° (9.5°, 106)	128.1° (10.1°, 106)

<sup>1</sup>No significant difference between groups ( $\chi^2=1.96$ ,  $p=0.5802$ ).

<sup>2</sup>Groups differ significantly ( $\chi^2=9.80$ ,  $p=0.0203$ ). Post-hoc testing revealed significant differences between australopith and early *Homo* samples, and between australopith and *H. sapiens* samples.

and equal variance across samples. Post hoc testing was done using the Tukey-Kramer honestly significant difference (HSD) test. All statistical treatments were conducted in JMP 8.0.2 (JMP 2009).

### COMPARATIVE MORPHOLOGY

Based on the preserved portion of the superior ilium in both MH1 and MH2, *Au. sediba* had an iliac blade with moderate sigmoid curvature to the iliac crest, bounding a relatively deep fossa for *M. gluteus medius* externally and a moderate *M. iliacus* fossa internally. The anterior portion of the preserved iliac crest curves medially, indicating a medially displaced ASIS, as is common in *Homo* (Rose 1984). Comparative groups do not differ significantly in the iliac crest posterior angle (ICPA: at the spina limitans), yet do differ significantly in mean values of the iliac crest anterior angle (ICAA: at the cristal tubercle) (Table 2). Both early *Homo* and modern humans tend to have low ICAA values, which serves to displace the ASIS medially relative to the morphology seen in most australopiths. The early *H. erectus* specimen KNM-WT 15000 is an exception in this regard (with an ICAA [175.9°] above that of the australopiths), although our measure of his ICAA is based on the heavily reconstructed left os coxae (Walker and Ruff 1993), and this reconstruction has been questioned (Arsuaga et al. 1999; Ruff 1995; Simpson et al. 2008). Removal of KNM-WT 15000 from the early *Homo* sample brings their mean ICAA value (129.8±9.1°, n=3) very close to the modern human mean, suggesting that reduction in the anterior angle is a derived feature in the genus *Homo*. Only two australopiths (with the exception of MH2)—A.L. 288-1 and Sts 14—have measurable ICAAs. However, a third specimen—StW 431—preserves the anterior half of the iliac crest and can be seen to have an ICAA that is more open than that of the other australopiths, which we estimate to be about 175°. Inclu-

sion of this estimate for StW 431 would bring the australopith sample mean to 171.3° (±3.8°, n=3). MH2 has an anterior angle value that is intermediate between the mean of the australopith sample and those of the two *Homo* samples (but with a sample n=1, this value is not significantly different from the medians of the other groups). Additional *Au. africanus* and *Au. robustus* specimens support the characterization of australopiths as having open anterior angles—SK 50, TM 1605, MLD 7 (juvenile), and Sts 65 all appear to share in having morphology suggestive of an open ICAA, including coronally-to-paracoronally oriented iliac blades, slight-to-moderate sigmoid curvature of the iliac crest, relatively shallow *M. iliacus* fossae, and slight medial deviation of the ASIS. However, two specimens—SK 3155b and MLD 25 (juvenile)—appear to have greater sigmoid curvature, deeper iliac fossae, and more medially positioned ASIS, and to have had ICAAs close to that observed in MH2.

Laterally flared iliac blades are characteristic of Pliocene hominins (Berge and Goularas 2010; Claxton et al. 2016; Haeusler 2002; Kibii and Clarke 2003; Lovejoy et al. 1973, 2009) and are thus considered a plesiomorphic trait for the genus *Homo* (Simpson et al. 2008) (but see VanSickle 2017 for a discussion of inconsistencies in how iliac flare has been defined and measured in hominin paleontology). Marked iliac flare is retained in early and middle Pleistocene *Homo* (Arsuaga et al. 1999; Simpson et al. 2008), and thus a reduction in this flaring may be an autapomorphic condition in *H. sapiens* (or one synapomorphically or homoplastically shared with Neandertals: see Rak and Arensburg 1987). Reduction in lateral flare is brought about, evolutionarily, by both an increase in sigmoid curvature (which serves to displace the ASIS medially) and a reorientation of the iliac blades from a paracoronary to a parasagittal position. Both of these shifts are reflected in the iliac angle formed between the superior pubic ramus and the anterior

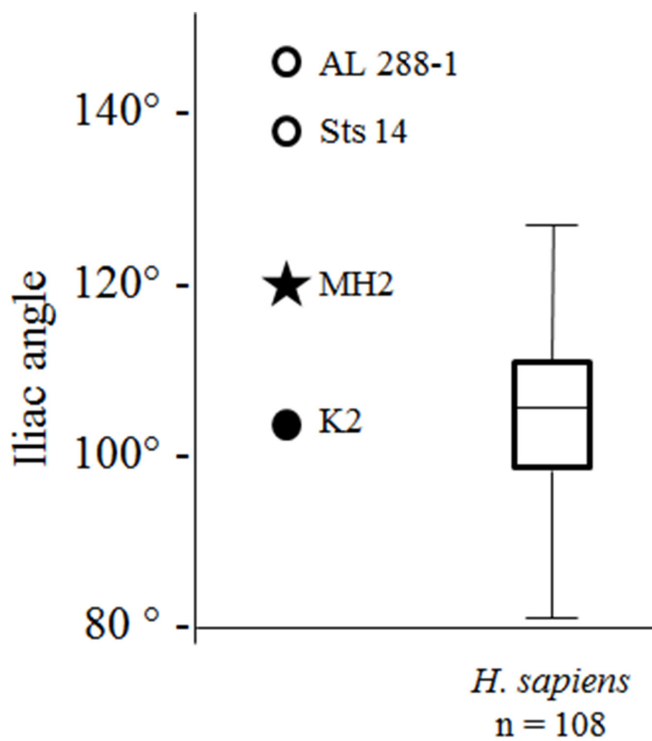


Figure 12. Iliac angle in MH2 compared to two australopiths (A.L. 288-1 and Sts 14), one representative of early *Homo* (Kerbarra 2), and *H. sapiens* ( $n=108$ ). Box-and-whiskers plot shows the median, upper and lower quantiles (box) and range (whiskers) for the *H. sapiens* sample. Kruskal-Wallis one-way analysis of variance detected a significant difference between groups ( $\chi^2=8.25$ ,  $p=0.0412$ ) and post-hoc testing revealed significant differences between the australopith sample and both the early *Homo* and *H. sapiens* samples (MH2 was not significantly different from any sample).

margin of the iliac blade (see Table 1). A conservative estimate of this angle in MH2 based on the preserved portion of the anterior iliac blade (see Kibii et al. 2011 SOM) is  $120^\circ$ , which falls well below the observed value of two australopiths and within the range of values in *H. sapiens* (Figure 12). As with our measure of sigmoid curvature of the iliac crest, the iliac angle of MH2 appears to be intermediate between the condition seen in other australopiths and that of *Homo*, although lack of adequate fossil sample sizes limits the confidence with which we can draw this inference.

The Malapa hominins are variable in their acetabulocrystal buttress (iliac pillar) morphology. MH1 has a distinct pillar that runs anterosuperiorly from the superior margin of the acetabulum. Although the buttress in MH1 is not as strongly developed as it is in some specimens that have been attributed to early *Homo* (such as KNM-ER 3228 and OH 28), its morphology is more similar to the morphology seen in early and modern *Homo* than it is to that of *Australopithecus*. MH2, on the other hand, lacks a distinct pillar, but rather exhibits an indistinct thickening of the anterior iliac blade, similar to the morphology seen in A.L. 288-1, Sts 14, and StW 431. Both specimens lack the ASIS

and the anterior iliac crest, and thus it is not possible to tell if the morphology of either specimen is best considered an acetabulocrystal buttress (that is, terminating in a distinct crystal tubercle on the iliac crest) or an acetabulospinous buttress (that is, terminating in the ASIS).

The acetabulosacral buttresses of the inferoposterior iliac body of both specimens appear robust compared to other australopiths. Since the rigidity of the buttress is inversely proportional to its length (the acetabulosacral load arm: ASLA [see Table 1]) and directly proportional to its minimum thickness (acetabulosacral buttress thickness: ASBT [see Table 1]), the ratio ASBT/ASLA serves as a convenient measure of its robusticity. As can be seen from Table 3, australopiths (as represented by specimens of *Au. afarensis*, *Au. africanus*, and *Au. robustus*) have gracile (non-robust) acetabulosacral buttresses, with mean ASBT/ASLA ratios that are 1.3 to 2.3 standard deviations below the mean values in the *Homo* samples. Australopiths have acetabulosacral buttresses that are thin for their length (Figure 13a), and robusticity indices that are small for their body size (using iliac breadth as a proxy for size: Figure 13b). MH1 and MH2 have some of the thickest buttresses among the australopith sample, and have high ASBT/ASLA ratios for their size relative to their congeners (a morphology that has been argued to reflect a change in loading dynamics in this region relative to the condition in earlier australopiths: Kibii et al. 2011). When acetabular diameter is used as a proxy for body size, australopiths appear to have both long ASLAs and moderately low ASBTs for their size (see Table 3), although it must be borne in mind that australopiths tend to have small femoral head (and thus acetabular) diameters for their body sizes (Ruff 2015). When iliac breadth is used instead, it appears that most australopiths (excluding the Malapa specimens) have moderately elongated ASLAs and very low ASBTs for their body size (Figure 13c and 13d).

Australopith ossa coxae are characterized by acetabular and auricular joint surfaces that are small relative to both body size and to those seen in most members of the genus *Homo* (Berge and Kazmierczak 1986; Churchill and VanSickle 2017). The Malapa hominins appear to fit the australopith pattern. In measures of absolute joint size (acetabular diameter and auricular surface area) MH1 and MH2 do not differ from a sample of other australopiths (including *Au. afarensis*, *Au. africanus*, and *Au. robustus*), but do differ significantly from samples of both early and recent *Homo* (Kibii et al. 2011 SOM). When either iliac breadth or the geometric mean of iliac dimensions are used to standardize acetabular and auricular size measures, *Au. sediba* is comparable to other australopiths, which in turn do not really differ from modern humans (Kibii et al. 2011 SOM). Early *Homo*, on the other hand, tends to distinguish itself in having large weight-bearing joint surfaces relative to iliac size (Kibii et al. 2011 SOM).

While the Malapa hominins may be australopith-like in the size of their coxal and sacroiliac joint surfaces, they appear (on the basis of the single preserved ischium of MH1) to be more *Homo*-like in length of the ischium and the atten-

**TABLE 3. MEAN (SD, N) ABSOLUTE AND RELATIVE ACETABULOSACRAL BUTRESS DIMENSIONS (mm) IN “CLASSIC” AND ROBUST AUSTRALOPITHS, SPECIMENS ATTRIBUTED TO EARLY *HOMO*, AND MODERN HUMANS.**

	ASLA	ASBT	ASBT/ASLA	ASLA/AD	ASBT/AD
<b>Australopiths<sup>1</sup></b>	48.2 (5.3, 3)	15.3 (1.2, 3)	0.32 (0.01, 3)	1.27 (0.26, 2)	0.41 (0.07, 2)
<b><i>Au. robustus</i><sup>2</sup></b>	49.8 (4.5, 3)	16.4 (2.2, 3)	0.33 (0.02, 3)	1.17 (0.03, 3)	0.38 (0.03, 3)
<b>early <i>Homo</i><sup>3</sup></b>	50.5 (6.3, 8)	22.0 (3.3, 8)	0.44 (0.09, 8)	0.87 (0.09, 8)	0.38 (0.06, 8)
<b>modern human females<sup>4</sup></b>	49.4 (5.5, 44)	20.7 (2.2, 45)	0.43 (0.08, 44)	1.04 (0.13, 44)	0.44 (0.04, 45)
<b>modern human males<sup>4</sup></b>	46.0 (5.6, 29)	24.0 (2.1, 29)	0.53 (0.09, 29)	0.89 (0.10, 29)	0.46 (0.04, 29)

Abbreviations: ASLA, acetabulosacral load arm; ASBT, acetabulosacral buttress thickness; AD, acetabular diameter.

<sup>1</sup>As represented by A.L. 288-1, Sts 14, and Sts 65.

<sup>2</sup>As represented by SK 50, SK 3155b, and TM 1605.

<sup>3</sup>Includes archaic *Homo* specimens (KNM-WT 15000, Kabwe E719 and E720, Arago XLIV, Kebara 2, and Krapina 207), as well as taxonomically uncertain specimens generally attributed to *Homo* (OH 28, and KNM-ER 3228).

<sup>4</sup>South African northern Nguni.

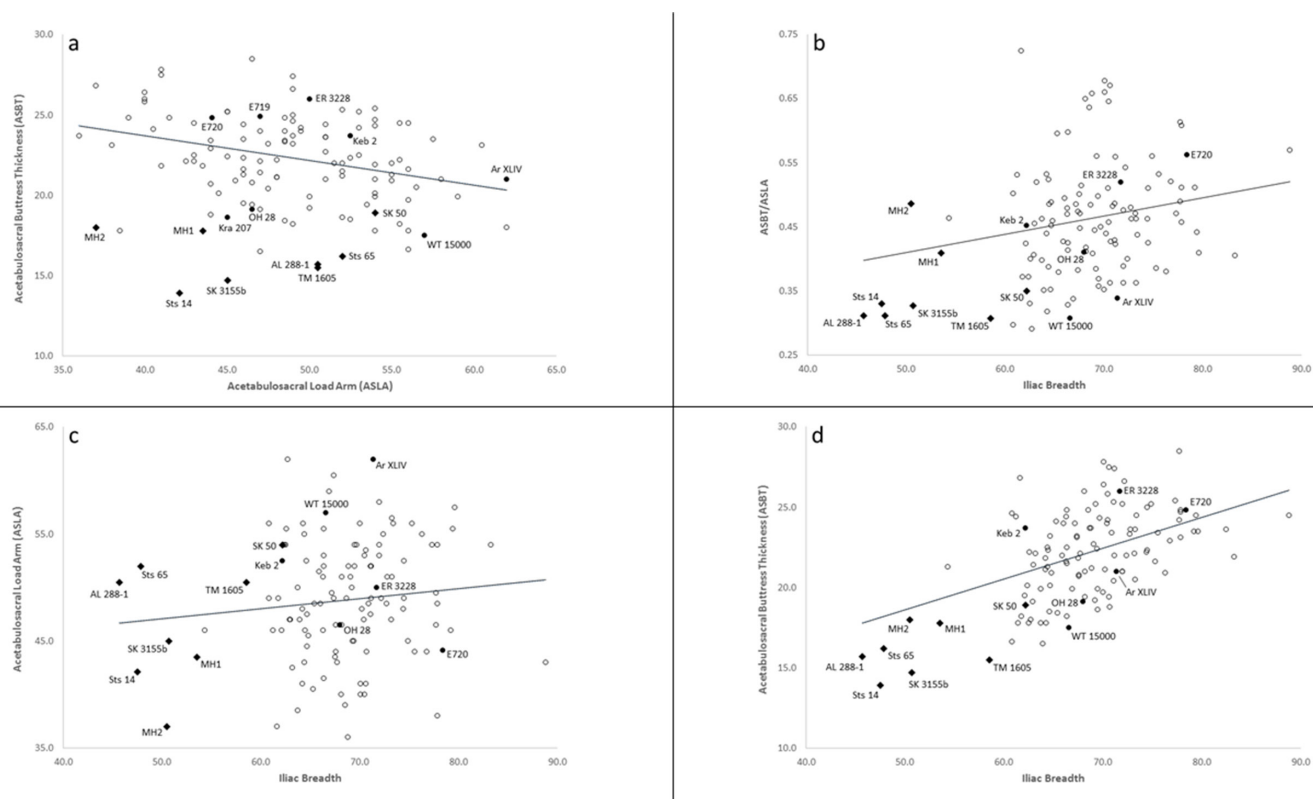


Figure 13. Relative acetabulosacral buttress dimensions in recent humans (open circles), australopiths (solid diamonds), and specimens attributed to early and archaic *Homo* (solid circles). All measurements in mm. Ordinary least squares (OLS) regression lines are provided for recent human sample only. a) ASBT vs. ASLA:  $y = -0.1536x + 29.854$ ;  $r = 0.3268$ . b) ASBT/ASLA vs. iliac breadth:  $y = 0.0028x + 0.2685$ ;  $r = 0.1746$ . c) ASLA vs. iliac breadth:  $y = 0.0938x + 42.3960$ ;  $r = 0.0938$ . d) ASBT vs. iliac breadth:  $y = 0.1918x + 9.0243$ ;  $r = 0.4165$ .

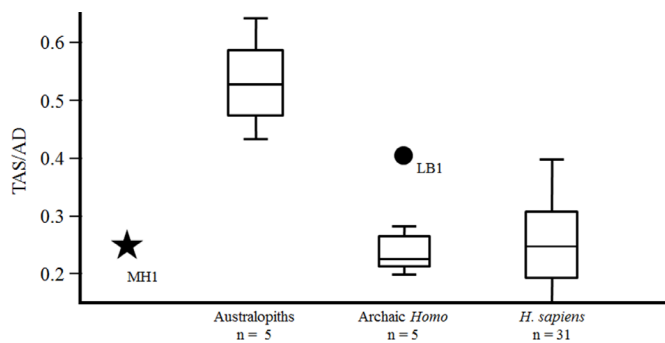


Figure 14. Relative tuberoacetabular sulcus diameter in MH1, *Australopithecus*, archaic *Homo*, and recent humans. Box-and-whiskers plots show the median, upper and lower quantiles (box) and range (whiskers). Data for LB1, representing *H. floresiensis*, from Jungers et al. (2009). See Kibii et al. (2011 SOM) for details about data collection from fossil specimens.

dant length of the moment arm of the hamstring muscles. Relative to body size (as represented by acetabular diameter), the hamstring moment arm (HMA: see Table 1) of MH1 (0.92) is small compared to australopithecus (1.19±0.06, n=3) but is not significantly different from our early *Homo* sample (0.99±0.04, n=5) (since the ontogenetic age of MH1 may be a factor, see discussion of MLD 8 below). While we did detect significant differences between groups in HMA/AD (chi-square=15.79, p=0.0013), we found that our australopithecus sample did not differ significantly from our recent human sample (1.14±0.09, n=74), although both differ significantly from *Au. sediba* and early *Homo*. Our recent human sample mean is considerably higher than that reported by Stern and Susman (1983) for a sample of 98 modern humans (1.056±0.07), whose data make it appear that the derived condition (seen in early *Homo* and *H. sapiens*, and shared by *Au. sediba*) is to have a short ischium with reduced leverage of the hamstring muscles. At present we do not know if the differences between our data and those of Stern and Susman (1983) is a function of different samples with different mechanical properties in the pelvis, measurement error, or sampling error. With respect to the minimum width of the tuberoacetabular sulcus (TAS: see Table 1), the same results obtain whether absolute or relative (TAS/AD) values are compared. In both dimensions, the australopithecus exhibit substantially longer ischia than any other group (Figure 14). Both comparisons produced significant chi-square statistics (TAS: 11.41, p=0.0097; TAS/AD: 13.28, p=0.0041), and post-hoc tests show the australopithecus sample to be significantly different from *Au. sediba*, early *Homo*, and modern *Homo* (with no significant differences between any of the latter three samples). Given the clear differences in TAS between australopithecus on the one hand and the Malapa/*Homo* specimens on the other, the more equivocal results of the HMA comparisons appear all the more puzzling, and suggest that the size of the ischial tuberosity itself may have a substantial impact on overall hamstring moment arm length. Regardless, based

on the morphology seen in MH1, *Au. sediba* appears to have had a *Homo*-like configuration of its hamstring origins (see Figure 14). Interestingly, the relative size of the tuberoacetabular sulcus in LB1 (the type specimen of *H. floresiensis*) is large compared to *Au. sediba* and specimens of early *Homo*, and even relative to most modern humans (see Figure 14). Although not as wide (relative to acetabular diameter) as specimens of *Au. afarensis* and *Au. africanus*, the tuberoacetabular sulcus of LB1 does look remarkably primitive, consistent with several other features noted in the LB1 pelvis (Churchill and VanSickle 2017; Jungers et al. 2009).

It has been suggested that some of the difference in relative ischial length between australopithecus and *Homo* (in TAS/AD) is a consequence of expansion of the diameter of the acetabulum in *Homo* (Haile-Selassie et al. 2010). This appears not to be the case for MH1, since its acetabulum is the same size as that of A.L. 288-1, and smaller than all the other australopithecus, yet its absolute and relative ischial length is *Homo*-like. Finally, it might be argued that, as a juvenile, MH1 had not attained full growth of the ischium, and that as an adult its morphology would be similar to that of other australopithecus. While we cannot as yet rule this possibility out, it bears noting that the juvenile *Au. africanus* specimen MLD 8 from Makapansgat, despite being of a considerably younger age-at-death than MH1 (based on overall size and the associated MLD 8 maxilla), already has a TAS that exceeds by 19% the width of MH1. It thus seems likely that the wide TAS characteristic of australopithecus was expressed at a young ontogenetic age, and that the morphology of MH1 would not have changed significantly with further growth.

The MH2 sacrum is like that of modern humans in having five sacral vertebrae, most likely in conjunction with five lumbar vertebrae (Williams et al. 2013). Also as in modern humans but unlike other australopithecus, the auricular surface extends onto the third sacral vertebrae. The size of the sacral centrum falls between those of smaller specimens of *Au. africanus* (Sts 14) and *Au. afarensis* (A.L. 288-1), but appears small relative to larger individuals such as StW 431 (*Au. africanus*) and KSD-VP-1/1 (*Au. afarensis*).

The pelvic remains of MH1 and MH2 show that some features of the pelvis that are considered to be derived for the genus *Homo* evolved at least once in the absence of encephalization and/or increased body size (Kibii et al. 2011). While the pelvis of *Au. sediba* still retains some primitive features (such as relatively long pubic rami, wide sacral alae, wide bi-acetabular diameter, and a marked angle between the facets for the hamstring muscles and adductor magnus on the ischial tuberosity), the overall pelvic architecture of the Malapa hominins is more like that of modern humans than it is of other australopithecus of similar body and brain size. Derived features in the pelvis of *Au. sediba* include parasagittally-oriented iliac blades with marked sigmoid curvature, greater robusticity of the acetabulocrystal buttress (in MH1; MH2 has the australopithecus condition of a weakly developed, indistinct iliac pillar), greater robusticity of the acetabulosacral buttress, an expanded retroauricular area with a pronounced iliac tuberosity, and a short

ischium with a narrow tuberoacetabular sulcus (Kibii et al. 2011). Given the small adult brain size inferred for *Au. sediba* (420–440 cc: Berger et al. 2010; Carlson et al. 2011), contrasts with other australopiths in pelvic morphology appear not to be due to differences between groups in encephalization-related obstetric mechanics. Likewise, given general parity in adult body size between *Au. sediba* (34–36 kg: Holliday et al. 2018) and other australopiths (23–50 kg: Antón et al. 2014), the presence of derived features in the hip bones of the Malapa hominins is unlikely to be due to evolutionary increases in body size. Relatively primitive pelvic morphology in *H. floresiensis* (Brown et al. 2004; Jungers et al. 2009) and the recently-discovered *H. naledi* (Berger et al. 2015; VanSickle et al. 2018) makes it unlikely that the derived features of the pelvis that *Au. sediba* shares with most species of *Homo* are homologous (Churchill and VanSickle 2017), but are likely instead to represent homoplastic features that evolved independently in the two lineages.

#### ACKNOWLEDGEMENTS

We thank the South African Heritage Resource agency for the permits to work at the Malapa site; the Nash family for granting access to the Malapa site and continued support of research on their reserve; the South African Department of Science and Technology, the South African National Research Foundation, the Institute for Human Evolution, University of the Witwatersrand, the Palaeontological Scientific Trust, the Andrew W. Mellon Foundation, the U.S. Diplomatic Mission to South Africa, the A.H. Schultz Foundation, the National Geographic Society, and Sir Richard Branson for funding; the University of the Witwatersrand's Schools of Geosciences and Anatomical Sciences and the Bernard Price Institute for Palaeontology for support and facilities; the Gauteng Government, Gauteng Department of Agriculture, Conservation and Environment, and the Cradle of Humankind Management Authority. For access to comparative specimens, E. Mbua, P. Kiura, V. Iminjili, and the National Museums of Kenya, B. Billings, B. Zipfel, and the School of Anatomical Sciences at the University of the Witwatersrand, and S. Potze, L.C. Kgasi, and the Ditsong Museum. For technical and material support, Optech and Optron; Duke University; and the University of Zurich 2009 and 2010 Field Schools. Numerous individuals were involved in the ongoing preparation and excavation of these fossils, including C. Dube, C. Kemp, M. Kgasi, M. Languza, J. Malaza, G. Mokoma, P. Mukanela, T. Nemvhundi, M. Ngcamphalala, S. Jirah, S. Tshabalala, and C. Yates. Other individuals who have given significant support to this project include B. de Klerk, C. Steininger, B. Kuhn, L. Pollarolo, B. Zipfel, J. Kretzen, D. Conforti, J. McCaffery, C. Dlamini, H. Visser, R. McCrae-Samuel, B. Nkosi, B. Louw, L. Backwell, F. Thackeray, and M. Peltier. J. Smilg facilitated computed tomography scanning of the specimens. We also thank two anonymous reviewers for helpful suggestions on an earlier draft of this paper.

#### REFERENCES

Abitbol, M.M. 1987. Evolution of the lumbosacral angle.

- American Journal of Physical Anthropology* 72, 361–372.
- Aiello, L.C. and Dean, M.C. 1990. *An Introduction to Human Evolutionary Anatomy*. Academic Press, London.
- Antón, S.C., Potts, R., and Aiello, L.C. 2014. Evolution of early *Homo*: An integrated biological perspective. *Science* 345, e1236828.
- Arsuaga, J.-L., Lorenzo, C., Carretero, J.-M., Gracia, A., Martínez, I., García, N., Bermúdez de Castro, J.-M., and Carbonell, E. 1999. A complete human pelvis from the Middle Pleistocene of Spain. *Nature* 399, 255–258.
- Arsuaga, J.L. and Alonso, J. 1983. Sexual variability and taxonomical variability in the innominate bone of *Australopithecus*. *Zeitschrift für Morphologie und Anthropologie* 73, 297–308.
- Berge, C. and Goullaras, D. 2010. A new reconstruction of Sts 14 pelvis (*Australopithecus africanus*) from computed tomography and three-dimensional modeling techniques. *Journal of Human Evolution* 58, 262–272.
- Berge, C. and Kazmierczak, J.-B. 1986. Effects of size and locomotor adaptations on the hominid pelvis: evaluation of australopithecine bipedality with a new multivariate method. *Folia Primatologica* 46, 185–204.
- Berger, L.R., de Ruiter, D.J., Churchill, S.E., Schmid, P., Carlson, K.J., Dirks, P.H.G.M., and Kibii, J.M. 2010. *Australopithecus sediba*: a new species of *Homo*-like australopithecine from South Africa. *Science* 328, 195–204.
- Berger, L.R., Hawks, J., de Ruiter, D.J., Churchill, S.E., Schmid, P., Deleuzene, L.K., Kivell, T.L., Garvin, H.M., Williams, S.A., DeSilva, J.M., Skinner, M.M., Musiba, C.M., Cameron, N., Holliday, T.W., Harcourt-Smith, W., Ackermann, R.R., Bastir, M., Bogin, B., Bolter, D., Brophy, J., Cofran, Z.D., Congdon, K.A., Deane, A.S., Dembo, M., Drapeau, M., Elliott, M.C., Feuerriegel, E.M., Garcia-Martinez, D., Green, D.J., Gurtov, A., Irish, J.D., Kruger, A., Laird, M.F., Marchi, D., Meyer, M.R., Nalla, S., Negash, E.W., Orr, C.M., Radovic, D., Schroeder, L., Scott, J.E., Throckmorton, Z., Tocheri, M.W., VanSickle, C., Walker, C.S., Wei, P., and Zipfel, B. 2015. *Homo naledi*, a new species of the genus *Homo* from the Dinaledi Chamber, South Africa. *eLife* 4, e09560.
- Bräuer G. 1988. Osteometrie. In *Anthropologie, Handbuch des vergleichenden Biologie des Menschen*, Band 1, Knussmann, R. (ed.). Gustav Fischer Verlag, Stuttgart, pp. 160–232.
- Brooks, S. and Suchey, J.M. 1990. Skeletal age determination based on the os pubis: a comparison of the Acsádi-Nemeskéri and Suchey-Brooks methods. *Human Evolution* 5, 227–238.
- Bruzek, J. 2002. A method for visual determination of sex, using the human hip bone. *American Journal of Physical Anthropology* 117, 157–168.
- Carlson, K.J., Stout, D., Jashashvili, T., de Ruiter, D.J., Tafforeau, P., Carlson, K., and Berger, L.R. 2011. The endocast of MH1, *Australopithecus sediba*. *Science* 333, 1402–1407.
- Churchill, S.E. and VanSickle, C. 2017. Pelvic morphology in *Homo erectus* and early *Homo*. *Anatomical Record* 300, 964–977.

- Claxton, A.G., Hammond, A.S., Romano, J., Oleinik, E., and DeSilva, J.M. 2016. Virtual reconstruction of the *Australopithecus africanus* pelvis Sts 65 with implications for obstetrics and locomotion. *Journal of Human Evolution* 99, 10–24.
- Day, M.H. 1971. Postcranial remains of *Homo erectus* from bed IV, Olduvai Gorge, Tanzania. *Nature* 232, 383–387.
- DeSilva, J.M., Holt, K.G., Churchill, S.E., Carlson, K.J., Walker, C.S., Zipfel, B., and Berger, L.R. 2013. The lower limb and the mechanics of walking in *Australopithecus sediba*. *Science* 340, 1232999.
- Dobson, S.D. 2005. Are the differences between Stw 431 (*Australopithecus africanus*) and A.L. 288-1 (*A. afarensis*) significant? *Journal of Human Evolution* 49, 143–154.
- Gommery, D., Senut, B., and Keyser, A.W. 2002. A fragmentary pelvis of *Paranthropus robustus* of the Plio-Pleistocene site of Drimolen (Republic of South Africa). *Geobios* 35, 265–281.
- Haeusler, M. 2002. New insights into the locomotion of *Australopithecus africanus* based on the pelvis. *Evolutionary Anthropology* Supplement. 1, 53–57.
- Haile-Selassie, Y., Latimer, B.M., Alene, M., Deino, A.L., Gibert, L., Melillo, S.M., Saylor, B.Z., Scott, G.R., and Lovejoy, C.O. 2010. An early *Australopithecus afarensis* postcranium from Woranso-Mille, Ethiopia. *Proceedings of the National Academy of Sciences* 107, 12121–12126.
- Hammond, A.S., Almécija, S., Libsekal, Y., Rook, L., and Macchiarelli, R. 2018. A partial *Homo* pelvis from the Early Pleistocene of Eritrea. *Journal of Human Evolution* 123, 109–128.
- Holliday, T.W., Churchill, S.E., Carlson, K.J., DeSilva, J.M., Schmid, P., Walker, C.S., and Berger, L.R. 2018 (this volume). Body size and proportions of *Australopithecus sediba*. *PaleoAnthropology* 2018, 406–422.
- İşcan, M.Y. and Steyn, M. 2013. *The Human Skeleton in Forensic Medicine*. 3rd edition. Springfield IL: Charles C Thomas.
- JMP 2009. Version 8.0.2. SAS Institute Inc., Cary, NC.
- Johanson, D.C., Lovejoy, C.O., Kimbel, W.H., White, T.D., Ward, S.C., Bush, M.E., Latimer, B.M., and Coppens, Y. 1982. Morphology of the Pliocene partial hominid skeleton (A.L. 288-1) from the Hadar Formation, Ethiopia. *American Journal of Physical Anthropology* 57, 403–451.
- Jungers, W.L., Larson, S.G., Harcourt-Smith, W., Morwood, M.J., Sutikna, T., Awe Due, R., and Djubiantono, T. 2009. Descriptions of the lower limb skeleton of *Homo floresiensis*. *Journal of Human Evolution* 57, 538–554.
- Kibii, J.M., Churchill, S.E., Schmid, P., Carlson, K.J., Reed, N.D., de Ruiter, D.J., and Berger, L.R. 2011. A partial pelvis of *Australopithecus sediba*. *Science* 333, 1407–1411.
- Kibii, J.M. and Clarke, R.J. 2003. A reconstruction of the Stw 431 *Australopithecus* pelvis based on newly discovered fragments. *South African Journal of Science* 99, 225–226.
- Lovejoy, C.O., Heiple, K.G., and Burstein, A.H. 1973. The gait of *Australopithecus*. *American Journal of Physical Anthropology* 38, 757–780.
- Lovejoy, C.O., Latimer, B.M., Spurlock, L., and Haile-Selassie, Y. 2016. The pelvic girdle and limb bones of KSD-VP-1/1. In *The Postcranial Anatomy of Australopithecus afarensis: New Insights from KSD-VP-1/1*, Haile-Selassie, Y. and Su, D.F. (eds.). Springer, Dordrecht, pp. 155–178.
- Lovejoy, C.O., Suwa, G., Spurlock, L., Asfaw, B., and White, T.D. 2009. The pelvis and femur of *Ardipithecus ramidus*: the emergence of upright walking. *Science* 326, 71e71–71e76.
- Martin, R. 1928. *Lehrbuch der Anthropologie*. Verlag von Gustav Fischer, Jena.
- Maass, P. and Friedling, L.J. 2016. Scars of parturition? Influences beyond parity. *International Journal of Osteoarchaeology* 26, 121–131.
- Ponseti, I.V. 1978. Growth and development of the acetabulum in the normal child: Anatomical, histological, and roentgenographic studies. *Journal of Bone and Joint Surgery* 60-A, 575–585.
- Rak, Y. and Arensburg, B. 1987. Kebara 2 Neanderthal pelvis: first look at a complete inlet. *American Journal of Physical Anthropology* 81, 323–332.
- Robinson, J.T. 1972. *Early Hominid Posture and Locomotion*. University of Chicago Press, Chicago.
- Rose, M.D. 1984. A hominine hip bone, KNM-ER 3228, from East Lake Turkana, Kenya. *American Journal of Physical Anthropology* 63, 371–378.
- Ruff, C.B. 1995. Biomechanics of the hip and birth in early *Homo*. *American Journal of Physical Anthropology* 98, 527–574.
- Ruff, C.B. 2015. The effects of hip joint loading on body mass estimation in early hominins. *American Journal of Physical Anthropology* Supplement 60, 273 (abstract).
- Simpson, S.W., Quade, J., Levin, N.E., Butler, R., Dupont-Nivet, G., Everett, M., and Semaw, S. 2008. A female *Homo erectus* pelvis from Gona, Ethiopia. *Science* 322, 1089–1092.
- Stern, J.T.J. and Susman, R.L. 1983. The locomotor anatomy of *Australopithecus afarensis*. *American Journal of Physical Anthropology* 60, 279–317.
- Stewart TD. 1970. Identification of the scars of parturition in the skeletal remains of females. In *Personal Identification in Mass Disasters*, Stewart, T.D. (ed.). Smithsonian Press: Washington, DC, pp. 127–135.
- Stringer, C.B. 1986. An archaic character in the Broken Hill innominate E.719. *American Journal of Physical Anthropology* 71, 115–120.
- VanSickle, C. 2017. Measuring lateral iliac flare by different methods risks obscuring evolutionary changes in the pelvis. *Anatomical Record* 300, 956–963.
- VanSickle, C., Cofran, Z.D., Garcia-Martinez, D., Williams, S.A., Churchill, S.E. Berger, and L.R., Hawks, J. 2018. *Homo naledi* pelvic remains from the Dinaledi Chamber, South Africa. *Journal of Human Evolution* 125, 122–136.
- Walker, A.C. and Leakey, R.E. 1993. *The Nariokotome Skeleton*. Harvard University Press, Cambridge.
- Walker, A.C. and Ruff, C.B. 1993. The reconstruction of the pelvis. In *The Nariokotome Skeleton*, Walker, A.C. and Leakey, R.E. (eds.). Harvard University Press, Cambridge, pp. 221–233.
- Ward, C.V., Feibel, C.S., Hammond, A.S., Leakey, L.N.,

- Moffett, E.A., Plavcan, J.M., Skinner, M.M., Spoor, F., and Leakey, M.G. 2015. Associated ilium and femur from Koobi Fora, Kenya, and postcranial diversity in early *Homo*. *Journal of Human Evolution* 81, 48–67.
- Williams, S.A., Meyer, M.R., Nalla, S., García-Martínez, D., Nalley, T.K., Eyre, J., Prang, T.C., Bastir, M., Schmid, P., Churchill, S.E., and Berger, L.R. 2018 (this volume). The vertebrae, ribs, and sternum of *Australopithecus sediba*. *PaleoAnthropology* 2018, 156–233.
- Williams, S.A., Ostrofsky, K.R., Frater, N., Churchill, S.E., Schmid, P., and Berger, L.R. 2013. The vertebral column of *Australopithecus sediba*. *Science* 340, 1232996.